DEVELOPMENT OF THERMOELECTRIC THICK-FILMS VIA ELECTROPHORETIC DEPOSITION

By

POUYA AMROLLAHI

Bachelor of Science in Materials Science and Engineering

University of Tehran

Tehran, Iran

2012

Submitted to the Faculty of the
Graduate College of the
Oklahoma State University
in partial fulfillment of
the requirements for
the Degree of
MASTER OF SCIENCE
July, 2014

DEVELOPMENT OF THERMOELECTRIC THICK-FILMS VIA ELECTROPHORETIC DEPOSITION

Thesis Approved:

Dr. Lobat Tayebi

Thesis Adviser

Dr. Daryoosh Vashaee

Dr. Raj N. Singh

Dr. Ranji Vaidyanathan

ACKNOWLEDGEMENTS

This thesis would have not been possible without the help and support from many people. Firstly, I would like to thank my advisors, Dr. Lobat Tayebi and Dr. Daryoosh Vashaee. Their patience, enthusiasm and encouragement greatly benefited me and this research work to grow from the immaturity to what it is today.

I would like to thank my thesis committee, Dr. Raj N. Singh and Dr. Ranji Vaidyanathan for their constructive discussion and great support to this research.

I would also like to thank my professors and colleagues at Oklahoma State University who have been providing me great advice and many opportunities. Their insightful suggestions and encouragement have been a huge impetus for me to grow professionally and personally.

Last but not least, I would like to thank my mom, dad and my wife, Farzaneh, for their moral support and constant confidence in me. Words can never express how much I appreciate their unconditional love and support.

Name: POUYA AMROLLAHI

Date of Degree: JULY, 2014

Title of Study: DEVELOPMENT OF THERMOELECTRIC THICK-FILMS VIA ELECTROPHORETIC DEPOSITION

Major Field: MATERIALS SCIENCE AND ENGINEERING

Abstract: Technological advancements in the past few decades have led to major improvements in living conditions; but, these improvements have come at a steep environmental price. Unsustainability, air pollution, greenhouse emissions, global warming, fragility of fossil-derived energy economies and sadly the yearly death rate of hundreds of thousands of people are the most important reasons that have forced the scientists and governments to think about novel renewable energies in order to solve the epic challenge of 21st century.

Among different forms of clean renewable energies, this thesis is dedicated to study thermoelectric power generation. Thermoelectric materials enable electrical power generation from the waste heat through a direct conversion, silent operation and low environmental load. These materials that operate at a wide range of temperatures and are easily scalable have relatively low efficiencies. Despite many progresses that have been made in bulk thermoelectric materials, there is still a lot of works to be done in fabrication of thermoelectric thin/thick-films.

This thesis studies fabrication and characterization of silicon germanium thermoelectric thick-films grown via electrophoretic deposition. Initial boron-doped SiGe/Glass powder was prepared though milling and in the electrophoretic deposition, Si wafer and sapphire discs have been used as the substrate. X-ray diffraction, scanning electron microscopy and laser scanning electron microscopy have been used for phase identification, morphology studies and surface topography, respectively. Seebeck coefficient and electrical conductivity were measured by the commercially available equipment; while the thermal conductivity of the films was measured by a laser flash unit. At last, TE figure-of-merit (ZT) was calculated.

TABLE OF CONTENTS

LIST OF TABLES

Table Page

LIST OF FIGURES

Figure Page

CHAPTER 1

Introduction and Literature review

1.1.Thermoelectric technology

Energy harvesting materials are the group of materials through which energy is derived from external sources (e.g. solar power, thermal energy, wind energy, salinity gradients, and kinetic energy), captured and stored for industrial applications [1]. As an important group of these materials, there has been a lot of attention in development and modification of thermoelectric (TE) materials for electronic refrigeration and power generation applications [2].

The discovery of basics and fundamentals of thermoelectrics dates back to mid-18th century. Beginning from early 1990s, environmental concerns and the energy crisis in the world led to novel scientific activities; which thereupon resulted in establishment of TE technologies [3]. Since then, there has been a growing interest in TE materials in many fields, such as space sciences [4], solar energy conversion [5] and microprocessors cooling [6]. However, to date, TE materials have found little commercial and industrial applications due to their low efficiencies [7]. Introduction of the concept of dimensionless TE figure-of-merit (ZT) [8] promoted the search for efficient TE materials. ZT, which correlates electrical conductivity (σ), Seebeck coefficient (S) and overall thermal conductivity (κ), is defined as,

$$ZT = \frac{\sigma S^2}{\kappa} \quad (1)$$

The measured thermal conductivity (κ) is an accumulation of electronic contribution (κ_e) and lattice contribution (κ_l). If the temperature difference is given, the materials ability to produce power can be evaluated by the term σS^2 which is called the Power Factor (PF). A good TE material has high σ (like metals), high S and low κ (like glass) [9]. S, σ and κ_e are functions of carrier concentration and chemical potential [10]. Hence, a better ZT is achievable either through optimization of carrier concentration or reducing the lattice component of K. Reduction of grain size, introduction of randomness and phonon scattering centers and utilization of several solid solutions and novel structures (such as superlattices and nano-wires) are the most recent strategies for maximizing ZT values [11, 12, 13, 14, 15]. Most of these attempts were based upon the reduction in κ_l values.

Silicon germanium alloys (SiGe) have been known as a TE material with high performances at high temperatures. This alloy offer the possibility of efficient TE generation from materials which are compatible with existing Si-based information and communication technologies [16] and the reduced dimensionality of quantum well structures lead to the possibility of improved TE properties with respect to bulk elemental or compound semiconductors [17].

Electrical properties of both p-type and n-type semiconducting materials can be indirectly affected though doping with an appropriate dopant via introducing and creating

acceptor and donor allowed energy states and shifting the energy bands relative to the Fermi level [18]. For silicon germanium alloys, boron is the material of choice as the dopant [9].

1.2.Thermoelectric Thin-films and Thick-films

Thin-film TE materials offer a significant scope for ZT enhancement [19]. For example, it is considered that the performance of Si/Ge thin-films can be improved and they can be employed as infrared sensors [20]. Bulk TE materials have been widely investigated in past few decades, due to their potency in playing a role in the epic energy challenge solution. Despite the recent progress that has been made in developing more efficient bulk TE materials, there are still several major obstacles remaining in the path of using the ordinary vacuum or non-vacuum TE device fabrication techniques for TE thin/thick-films.

TE thin/thick-films must have [21, 22]:

i. Thickness of more than tens of micron (governed by the fact that resistance of the ohmic contact must be much more smaller than the resistance of the TE element);
ii. Smooth and flat surface with the minimum possible roughness (obliged by module fabrication criteria).

Both vacuum and non-vacuum deposition techniques have been used for production of thick-films. However, vacuum deposition methods are more costly and non-vacuum

deposition methods such as spray pyrolysis, screen/inkjet printing and electroplating encounter various technical obstacles [23, 24, 25]. Recently, there has been a growing interest in using electrophoretic deposition (EPD) in the TE film fabrication process [26, 27, 28, 29].

1.3.Electrophoretic deposition (EPD)

EPD is a material processing technique using deposition of charged particles in a stable colloidal suspension on a conductive substrate, acting as one of the two oppositely charged electrodes in the EPD cell. The deposited particles form the intended material or device [30]. Both alternating current (AC) and direct current (DC) electrical fields have been applied in EPD process, although DC fields are more common [30, 31, 32]. Highly versatile application, simple apparatus and equipment, short processing time, cost effectiveness, facile modification, desirable dense packing of particles in the final piece, high quality of the microstructures produced, easy production of geometrically complicated shapes, and simple control of the thickness and morphology have made EPD an interesting technique both in academia and industry [30, 33]. In EPD, the state of particles in suspension and their evolution during the process can be controlled and manipulated. Moreover, appropriate and accurate choice of processing variables could enable production of dense and homogeneous or porous microstructures. A combustible substrate that can be removed by further heating in sintering process is used for fabricating complicated shapes. But for coatings, the operator needs to be very cautious

about possible cracks due to drying and sintering. These thermally derived cracks are the impartible nature of the technique and the quality of the final surface depends on overcoming this problem.

This process was discovered by Bose in a liquid-siphon experiment during the 1740s [34] and has been known since Ruess observed the movement of clay particles in water under an electrical field [35]. The first practical use of this technique was done by Harsanyi [36] in 1927 in order to deposit thoria (thorium (IV) oxide) and tungsten on a platinum cathode as an emitter for electron tube applications. The first large scale application of EPD dates back to early 1950s, when the scientists used this method to make insulating Al_2O_3 layers on cathode heaters in vacuum tubes [37].

An EPD cell contains four different parts: working electrodes (substrate and counter electrode), colloidal suspension, and power supply (AC or DC).

Despite the fact that many mechanisms have been proposed for EPD, there are several unquestionable characteristics to distinguish EPD from other similar deposition-based techniques. As it can be seen in Figure 1, (a) colloidal particles are well dispersed and able to move freely and independently in solvent suspension, (b) electrochemical equilibrium of the solvent is responsible for particles' surface charge, (c) particles move electrophoretically in the bulk of the suspension to the oppositely charged electrode (substrate) and (d) the substrate is covered by a neutralized firmly deposited layer of particles. Therefore, EPD is a technique where moving species are solid particles, required conductance of the liquid medium is low, and the organic liquids are preferred.

In EPD the liquid stays motionless while particles and ions move under the electrostatic force [33].

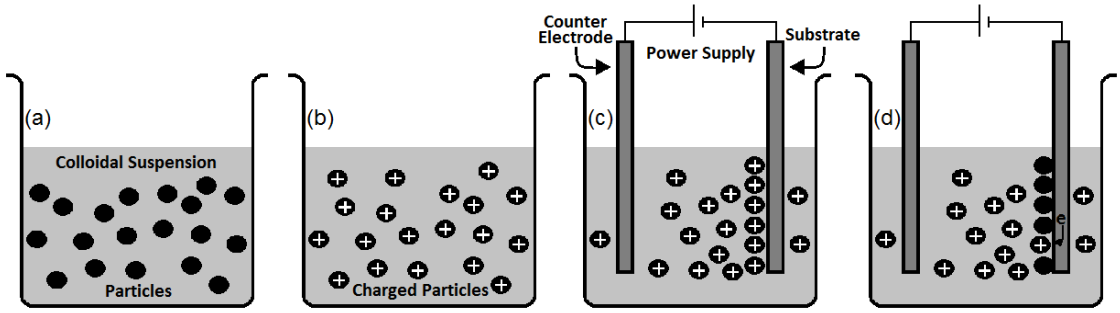

Figure 1 - 4 steps of EPD; (a) dispersion, (b) electrochemical charging, (c) electrophoresis and (d) deposition.

Like in any other system, it is absolutely essential to avoid contamination or impurity that can unfavorably influence the properties of the process and/or resulting materials. As the characteristics of the resulting materials are highly dependent on stability of suspension and control on surface charge, powder washing multiple times before preparation of a particulate suspension is mandatory in order to eliminate the residual impurities caused by the powder preparation procedure [38].

Generally, it is preferred to use organic liquids as the suspending medium in an EPD cell even though they are dangerous, expensive and unfriendly to the environment. However, in aqueous EPD, one needs much lower voltage, we have more control on temperature and deposition takes place faster. Also, water is much more environmental friendly. Unfortunately, electrolysis of water generates gas bubbles that drastically compromise the quality of the deposited layer. It has been reported that application of

short voltage pulses in an aqueous EPD system can suppress the bubble incorporation [39, 40]. Figure 2 demonstrates complete suppression of bubbles during aqueous electrophoresis of α-alumina thin-film, deposited on stainless steel (316L) substrate by applying periodically pulsed voltage. As can be seen, bubble free deposits were obtained at pulses equal to or shorter than 5 ms. It has also been reported that constant-current rather than constant voltage depositions are more efficient and can provide better control over the EPD process.

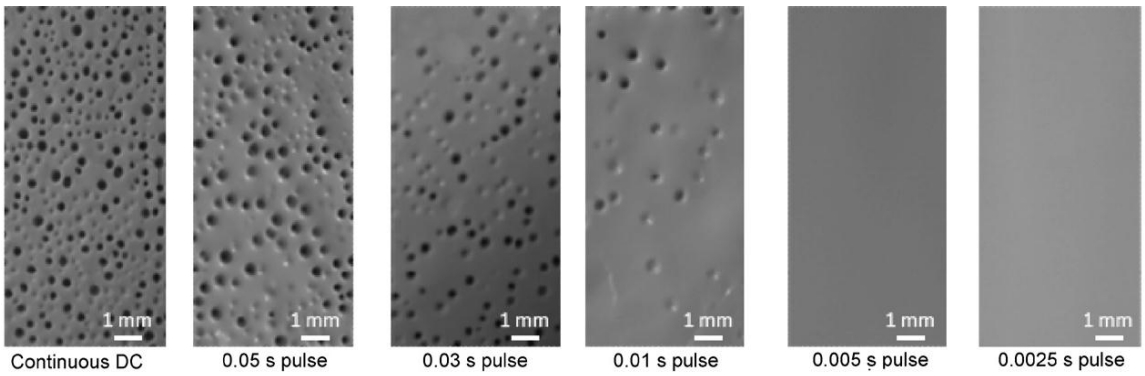

Figure 2 - Suppression of bubbles by applying constant current pulses. (α-alumina deposited on stainless steel substrates) [40].

Table 1 lists the reported applications of EPD in various fields:

Table 1 - Applications of EPD.

No.	Category	Application	Reference
1	Oriented ceramic materials	Fabricating crystalline oriented thick films	[56, 57, 58]
		Textured TiO_2	[15, 16, 17]
		Textured alumina	[18, 19]
2	Multilayered composites	Multi-layered alumina	[20]
		Fabricating functionally gradient, multi-layer composites and sandwich structures	[21, 22, 23]
3	Thermoelectric thick films	Si-Ge thick-films	[24]
4	Particle size separation	SnO_2 particles	[25]

5	Deposition of nanotubes	Graphene synthesis	[26, 27, 28]
		SiO_2/CNT composites	[29]
		CNT/TiO_2 composites	[30, 31]
		MnO_2/CNT composites	[32]
		Fe_3O_4/CNT composites	[33]
		Hydroxyapatite/CNT composites	[34, 35, 36]
		Bioactive glass/CNT composites	[37, 38]
6	Dye sensitized solar cells	Dye sensitized solar cells	[39, 40]
7	SiC fiber reinforced composites	SiC fiber reinforced composites	[41]
8	Thick film optical modulators	WO_3 nano rods	[42]
		ZnO thin films	[43]
9	Batteries and electrochemical capacitors	Lithium ion batteries	[44]
		Super-capacitors	[45]
10	Solid Oxide Fuel Cells	Y_2O_3-stabilized ZrO_2	[46, 47, 48, 49]
		Perovskite structures	[50]
		CeO_2 films	[51]
		Gd_2O_3	[52]
11	Corrosion-resistant Coatings	Silica hybrid coatings	[53]
12	Catalyst support and molecular sieves	PPy coated tubes	[54]
13	Sensors	Gas sensors	[55, 56, 57, 58]
14	Piezoelectric actuators	PZT actuators	[59, 60]
15	Biomedical materials	Forming biocompatible layers	[61, 62, 63, 64, 65, 66, 67, 68, 69, 70]
		Porous scaffolds	[71]
		Bacteria	[72]
		Corrosion protection of implants	[73]

EPD process contains 4 steps. First, a stable suspension of particles is needed. Since the particles only need to be stable within the time frame between dispersing to depositing processes, which can be as short as a few minutes, various stabilization techniques may be utilized such as low concentration, proper charging of the particles, polymer depletion, poly-electrolyte, block co-polymer, and homo-polymer adsorption

[41]. In electrostatic technique, creation of an energy barrier between 10 and 15 kT prevents the particles from attaching to each other. In polymer depletion, a concentration of soluble polymer which cannot be adsorbed to the particle surfaces is used to prevent them from sticking together. Other polymeric stabilization methods necessitate a polymer where one side of it can be attached to the particle, while the other side is dissolved in the solvent [41]. As the second step, a solvent able to enable ionic charge is required where adsorption/dissolution equilibria for a positive and negative ion are different. The next step is electrophoretic migration of particles under the influence of electric field. During electrochemical charging of particles, the solvent must be able to dissolve ions; because a solvent with no or a minute concentration of dissolved ions drastically increase the required voltage across the cell. Electrochemical reactions at the electrodes guarantee the change in the valence of ions in order to prevent ions from screening the electric field at the electrode surface. Moreover, absence of these reactions would lead to fast migration of ions to oppositely charged electrodes after applying a voltage.

The last step is deposition of particles on one of the electrodes. As there are various mechanisms for both stabilizing and destabilizing of the particles (in the first and fourth steps), there is no single mechanism for EPD.

1.3.1. Mechanisms

There are several mechanisms by which the particles come together and form a rigid solid structure. Combining them with the above mentioned dispersing techniques leads to

different EPD mechanisms although the exact mechanisms which allow deposition of particles on the substrate are still not completely understood.

It has been suggested that EPD should be considered as a two-step process, where particles first migrate to the substrate due to the applied electric field (the particles lose their charge at the electrode surface) and then after complex electrochemical reactions and aggregation the deposited layer is formed.

Electrophoretic motion of the particles is stopped by the substrate and the density of the particles will keep increasing there, due to accumulation. If those particles agglomerate, a low-density deposit may form which is difficult to dry without cracking. In this mechanism, there is no guarantee that the thickness of the layer remains uniform all over the substrate; since the non-uniformity of the electric field can lead to a very non-uniform deposit.

If the applied electric field is powerful enough (around several hundred volts per cm), it is also possible that deposition takes place via suppressing the electrostatic repulsion with the electric field. In this mechanism, the electrical force gradient has to be low in order to make an even deposit [42, 43], although some irregularities may occur due to strong electro-convection.

The next approach is flocculation of the particles by electro-sedimentation [41]. It was found that a stable suspension can produce strongly adhering sediment. Sediment is formed in the innermost layer of the particles due to gravitation plus the pressure made by electrically induced flow of particles to the substrate. Although the density of the

deposited layer is very good, the charge of the layer confronts the electrochemical charge of the solvent and acts as the driving force reducing the electrophoretic force in the layer. This instability can cause convection within the layer of particles before they are deposited on the substrate [44, 45].

Decrease in total ionic concentration around the substrate can raise the voltage gradient and, by quelling the convection, conduction occurs between unbalanced ions as a consequence. This effect results in raising the voltage gradient to mega volts per meter. These layers are very convectively unstable. Preservation of the surface charge of the particles results in a very strong compacting force that can make a powerful leveling effect when it is accompanied by high voltage gradient. This mechanism leads to forming very even thin layer [46].

On the contrary, it has also been reported that an increase in ionic concentration at the substrate makes the electrostatic boundary layer of particles thinner and thinner until they become unstable and the deposit is formed [47].

The particles may lose their charge and neutralize after contacting the substrate and make a thin deposit. This mechanism continues until the deposited layer gets thick, the particle-substrate interactions are stopped, or the pH level changes around the substrate [41].

It has been reported that repulsive forces between the particles can be reduced only when the electrode reactions generate $(OH)^-$ ions [33]. The calculated amount of ionic strength around the substrate was sufficient for flocculation of the suspension. Inter-

particle repulsion decreases when near-substrate electrolyte concentration is increased. Consequently, the zeta potential is lowered and flocculation of particles is induced.

In the case of polymers, it has been reported that when electrophoretic force brings the particles together, branches of a co-polymer can be detached from one particle and attach to a neighbor particle and make a polymer bridge that holds these particles together [41]. Another deposition mechanism for polymers is called "squeezing out", where a constant stable electrophoretic force brings two polymers into contact and deposit. Furthermore, in some cases, changing the solvent ionic composition leads to an alteration in particle surface potential and polymer particles can be stabilized [41]. Table 2 summarizes the mechanisms through which (a) particles stabilize at the substrate and (b) EPD takes place.

Table 2 - Mechanisms of EPD [74].

(a)	(b)
Low number density	Densification
Electrostatic	Direct electrostatic force
Polymer depletion	Electro-sedimentary
Homo-polymer adsorption	Ion depletion enhanced electrostatic
Poly-electrolyte	Desorption of neutral/charged polymer
Block co-polymer	Charge reduction/neutralization
	Squeezing out
	Bridging flocculation

1.3.2. Process variables

There are two sets of parameters which can affect both EPD process and the resulting specimen: first, parameters that control the status and quality of suspension, and then the parameters which qualify the whole process, such as electrical parameters. When the first group is fixed, the later can be manipulated for gaining favorable deposition. Table 3 summarizes the possible parameters that can be manipulated in order to get the desired properties and quality in the deposited film.

Table 3 - Parameters governing EPD.

Suspension Parameters	Process Parameters
Particle size Dielectric constant, conductivity and viscosity Zeta Potential Stability Concentration of solids	Applied electric field Deposition time Conductivity of the substrate

i. Suspension Parameters

- Particle Size

Uniformity of the deposited layer is tightly tied to whether or not the particles remain stable and dispersed throughout the whole process, because, motionless and accumulated particles lead to the formation of gradient in deposition. In case of larger particles, there

is always a competition between the gravity and electrophoresis forces. The first one result in sedimentation of the powder while the latter deposits the particles on the substrate. In this situation, when EPD is completed, surface charge is highly increased and/or the electrical double layer region is thickened.

- Dielectric Constant, Conductivity and Viscosity of Suspension

It has been reported that the dielectric constant of the liquids must be in the range of 12-25 for deposition to happen [30]. In liquids with dielectric constants less than 12, lack of dissociative power stalls the deposition, while in liquids with dielectric constants higher than 25, electrophoresis is halted by the reduction in size of the double layer region, caused by high ionic concentration.

Impurities can also change conductivity of the suspension. Moreover, the method used for preparing the suspension also affects the conductivity drastically. A highly-resistive suspension leads to instability because electronically originated charge forms in the particles. On the other hand, proper adjustment of temperature and dispersant concentration can raise the conductivity. Research has shown that, for each exact dispersant concentration and each temperature, there is a narrow conductivity range which enhances the deposition process [48]. Generally, an ideal suspension has high dielectric constant, low conductivity and low viscosity. Table 4 shows viscosity and relative dielectric constant of some popular solvents [49], ordered from best to worst. Methanol and acetone are the first two best solvents. However, comparing these two, methanol has higher dielectric constant while acetone has a viscosity of almost half of

methanol. Therefore, acetone can be considered as the best solvent for making an ideal suspension.

Table 4 - Physical properties of solvents used for EPD.

Solvents	Viscosity $(cP) = 10^{-3}\ N.s.m^{-2}$	Relative dielectric constant
Acetone	0.3087	20.7
Methanol	0.557	32.63
Water	0.890	78.2
Ethanol	1.0885	24.55
Acetylacetone	1.09	25.7
***n*-Propanol**	1.9365	20.33
Iso-propanol	2.0439	19.92
***n*-Butanol**	2.5875	17.51
Ethylene glycol	16.265	37.7

- Zeta Potential

Zeta potential governs several key parameters in EPD, such as the density of the deposit, particle direction and speed, and the repulsive interactions between the particles which determines the stability of the suspension. Generally, a high surface charge is needed not only to avoid particle agglomeration but also to enable formation of a dense highly-packed deposit. Zeta potential manipulation is done through addition of acids, bases and adsorbed ions.

- Stability of Suspension

Finding the best state of stability of the suspension is a matter of compromise. When the suspension is stable, flocculation does not happen and a thick adherent material deposits at the bottom of the cell due to sedimentation. Too much stability disables EPD,

because a high electric field is needed to defeat the repulsive forces between particles. Conversely, a flocculating suspension just forms thin non-adhering deposits.

- Concentration of Solids in Suspension

High concentrations of solids in suspension enable uniform and even deposition rates, while low concentrations lead to deposition rates proportional to electrophoretic mobility of each particle [50].

ii. Process Parameters

- Applied Electric Field

As there are both intended particles and free ions in the suspension, a portion of the electric field, which is the driving force of EPD, is carried by the free ions and the field efficiency is compromised. However, when we cannot limit the presence of free ions, the amount of current carried by them is insignificant. Ideally, the applied electric field must be totally spent on advancement of the electrophoresis in a stable-current manner, because the deposition increases in direct relation with raising the applied potential. While too low fields are not capable of triggering the electrophoresis, with too high applied electrical fields, the quality of the deposits is sacrificed. It has been suggested that the best quality of deposits are gained at moderate applied fields. Moreover, a high electric field can cause turbulence in the suspension, which compromises the quality of the resulting deposit. Also, it increases the speed of the particles and consequently they cannot have the chance to be seated in the best position, which makes the formation of a dense close-packed structure impossible [51].

- Deposition Time

In EPD, the deposition rate starts with a linear relationship to time and then it lowers as time goes on, until the deposit is thick enough to interrupt the conductance and the deposition rate reaches plateau at high deposition times.

- Conductivity of Substrate

In EPD, the quality of the deposited film is strongly dependent on the conductivity of the substrate. Low conductivity of the substrate leads to both slow deposition and non-uniformity of the deposit [52].

1.3.3. General applications

- Oriented ceramic materials

EPD has been given special attention as the leading ceramic electrodeposition technique in the last decades [53, 54]. This technique has revolutionized advanced ceramic materials processing both in academia and industry. In ceramic industries, thin ceramic films can be achieved from colloidal suspensions. In recent years, the attractive characteristics of EPD have made it a potential alternative approach for many purposes in several fields. For example, EPD has been reported as a promising technique for fabricating crystalline oriented thick-films [35, 55, 53, 56]. Titanium oxide that has three crystallographic polymorphs (anatase, rutile, and brookite) has been widely used in different areas due to its remarkable optical characteristics. In another study [57], it has been shown that EPD in a strong magnetic field enables taking advantage of magnetic

anisotropy of materials with asymmetric crystalline structures to produce layers of aligned crystalline magnetic particles. The crystal anisotropy produces the driving force (ΔF) of this magnetic alignment and it is described by equation (2) [58],

$$\Delta \boldsymbol{F} = \Delta \boldsymbol{\chi} \boldsymbol{V} \boldsymbol{B}^{\boldsymbol{2}} / \boldsymbol{2} \boldsymbol{\mu}_{\boldsymbol{0}} \qquad (2)$$

where $\Delta \boldsymbol{\chi}$ is the difference between susceptibilities parallel and perpendicular to the magnetic principal axis, V is the volume of the material, B is the applied magnetic field, and μ_0 is the permeability in a vacuum. Figure 3 depicts a schematic view of the EPD cell in this investigation.

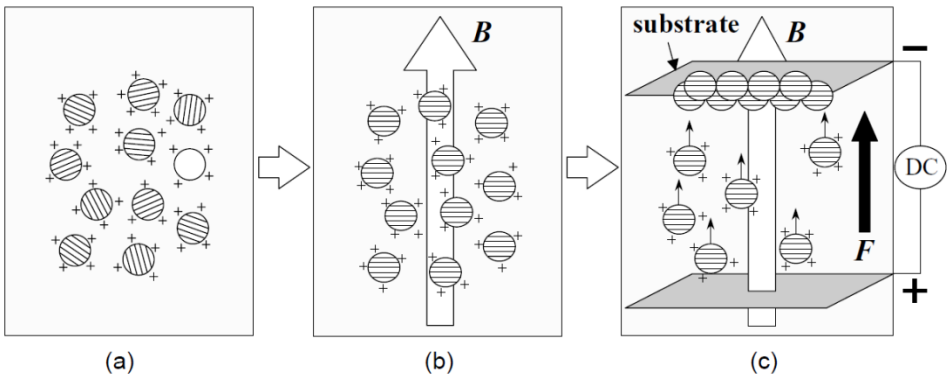

Figure 3 - Schematic view of EPD under high magnetic field; (a) suspension, (b) magnetic orientation and (c) preferred deposition *[56]*.

TiO_2 powder was sonicated in distilled water at pH 5.5, and then polyethylenimine (PEI) was added to improve stability of the suspension. PEI modified the zeta-potential of the powder. The EPD was done in presence of magnetic field at current density of 2.7 mA/cm^2. As a result, the magnetic field fixes the orientation of each particle and the

crystalline structure of polycrystalline TiO_2 can be controlled [57]. Figure 4 shows the XRD pattern of the top and side planes of the deposited anatase.

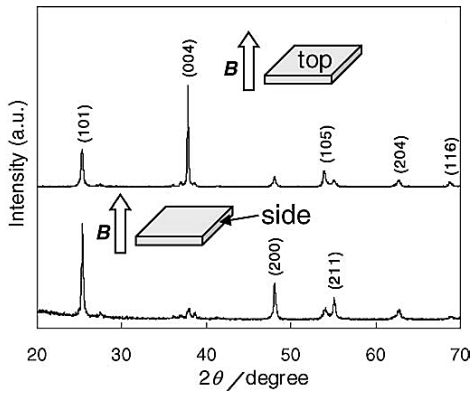

Figure 4 - XRD pattern of the top and side planes of deposited anatase *[57]*.

α-alumina is an interesting engineering material [57], possibility of fabrication of textured alumina by EPD was also investigated [59]. High purity fine α-alumina and hexagonal alumina platelets as matrix powder and template were used. The matrix powder was milled for 24 hours in ethanol and 0.5 vol.% de-ionized water. Platelets were then added to the suspension with n-butylamine and Dolapix Ce-64 (Dolapix is an anionic polyelectrolyte dispersant that contains ammonium salt of polymethacrylic acid [60]) in order to negatively charge and disperse the particles. The pH of the suspension was at 11.5 for the whole 450-second duration of the procedure. As a result, (001) alumina texture was obtained.

- Multilayered composites

Another group reported enhanced mechanical properties in textured, multi-layered alumina produced via EPD [61]. It has also been reported that EPD is capable of

fabricating functionally gradient and multi-layer composites and sandwich structures [62, 63, 64]. Functionally graded materials are advanced composite materials which consist of different layers with different mechanical properties and are able to alleviate problems associated with interfaces of different materials [65, 66]. Polycrystalline diamond has wide applications in for cutting and grinding in machining, mining and oil industries. Researchers have been successful in electrophoresis of diamond powder which was first acid washed and then boiled and rinsed in HCl solution and distilled water. Figure 5 shows a SEM image of diamond/diamond laminates formed by EPD of diamond powders with different concentrations in HCl solution. Direct-current EPD on tungsten carbide substrates was conducted at a constant voltage of 1.5 for 7.5 minutes for each layer [64]. Due to the high accuracy of EPD [30], sandwich-structured materials can be fabricated after several steps in both single-bath and multi-baths experiments [64].

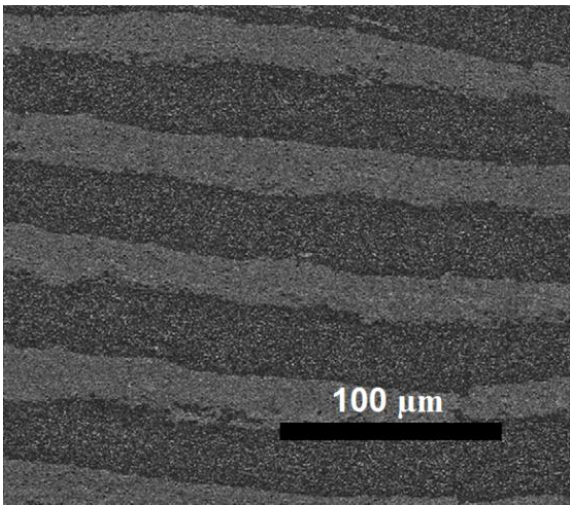

Figure 5 - SEM image of cross-section of diamond/diamond laminates *[64]*.

- Particle size separation

Particle size separation is another capacity of EPD [67]. In one investigation two parallel non-conductive electrodes were attached to borosilicate glass by gold paste. SnO_2 particles were dispersed in pure acetone and alternating-current EPD was done at 40 V for 10 minutes. It has been shown that increasing the frequency of the AC field leads to narrowing of the size distribution curve.

- Deposition of nanotubes

EPD has been used to improve carbon nanotubes (CNTs), to make CNT-composites and for graphene synthesis [68, 69, 70]. Various composites including SiO_2/CNT [71], CNT/TiO_2 [72, 73], MnO_2/CNT [74], Fe_3O_4/CNT [75], hydroxyapatite/CNT [76, 77, 78], and bioactive glass/CNT composites [79, 80] have been made using homogeneous dispersion of CNTs in an appropriate solvent. Fibers coated with single-walled CNTs, which can be used for extracting phenols from aqueous solutions, have also been prepared by electrophoresis of a suspension of CNTs in dimethylformamide at a constant voltage of 40 V for 10 seconds [81].

Figure 6 shows different outcomes of EPD made CNT/ceramic nanocomposites. Depending on the conditions sometimes ceramic or metallic particles are deposited on CNTs, in other cases CNTs are coagulated onto particles, and it is also possible to achieve simultaneous deposition of CNTs and particles.

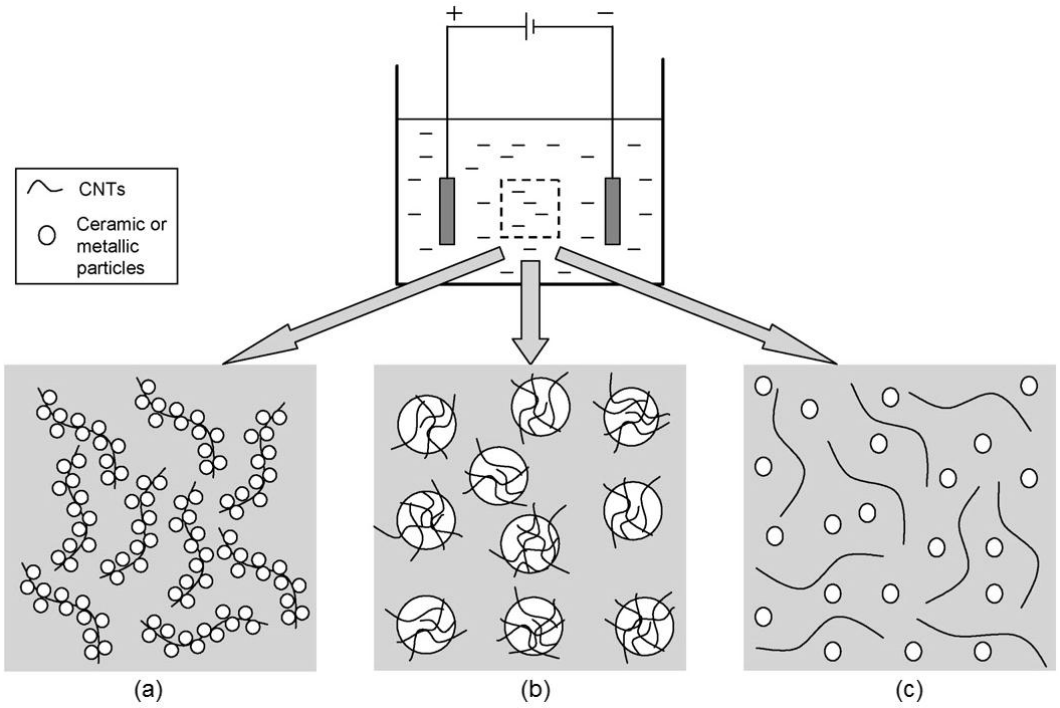

Figure 6 - Deposition of (a) particles on CNTs, (b) CNTs on particles, and (c) co-deposition of CNTs and particles *[68]*.

- Dye sensitized solar cells

Efficient dye sensitized solar cells (DSSCs) can be made through multiple EPDs [82, 83]. DSSCs are photovoltaic devices with high conversion efficiency [84] and their properties were modified after EPD at constant voltage of 10 V for 20 fifteen-second cycles at 25°C and further annealing (Figure 7-a). Figure 7-b shows the enhanced efficiency of these cells by increasing the number of the layers.

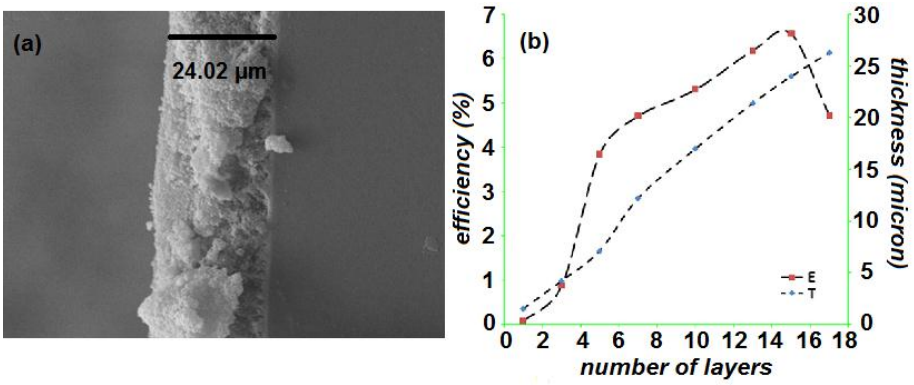

Figure 7 - (a) SEM image of cross-section of fabricated DSSC after annealing at 500 ˚C, (b) the effect of number of layers on thickness (T) and efficiency (E) of EPD fabricated DSSCs *[83]*.

- SiC fiber reinforced composites

SiC-fiber-reinforced composites have a great potential to be used for fusion reactors due to their remarkable resistance against neutron flux [85, 86]. EPD production of these composites [87] led to the idea that the quality and density obtained in this procedure is highly correlated with the zeta-potential of the charged particles. The experiment was conducted at constant voltage of 60 V for 5 minutes under DC electrical field. It has also been demonstrated that addition of both cationic deflocculant and Dolapix (a common deflocculant and dispersant in ceramic industry) and adjusting the pH around 9 improved the resulting properties.

- Thick-film optical modulators

WO_3 is used for optical modulation due to its electrochromic color [88]. Although hydrothermal process is the most popular technique for synthesis of tungsten oxide [89],

it needs several additional steps to complete the procedure; EPD has the significant advantage of having control over the whole process via manipulating pH level, process duration and electrical power [90]. In the experiment, nanorods of WO_3 were dispersed in de-ionized water with a pH level of around 6.77. Indium tin oxide glass (ITO-glass is a transparent conductive solid solution of In_2O_3 and SnO_2) was used as the working electrode with positive charge, and the process was done at a constant current of 0.8 mA/cm^2. Successful EPD of transparent ZnO thin-films has also been reported recently [91].

- Batteries and electrochemical capacitors

The ability of producing thick-films by EPD has made it interesting for application in lithium batteries [92] which currently are the most favorable portable energy source in electronic devices [93].

High power and long life cycle of electrochemical capacitors, which operate via taking advantage of the double-layer formed at the interface of electrode and electrolyte [94], have made them a promising choice for energy storage applications [95, 96]. The supercapacitor performance was significantly improved through EPD of hydrous ruthenium oxide particles with poly tetra-fluoroethylene (PTFE is a highly hydrophobic synthetic polymer) [97]. A schematic sketch of electrophoresis of these to particles can be seen in Figure 8-a; while Figure 8-b shows the increase in specific capacitance of electrodes coated with these materials as a function of loading weight for hydrous ruthenium oxide electrodes.

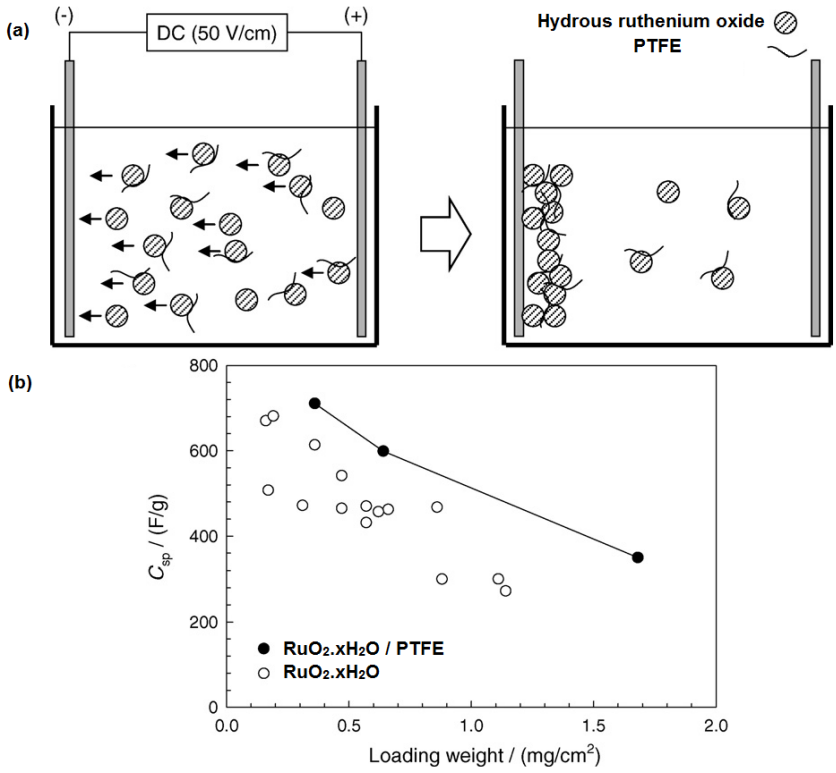

Figure 8 - (a) EPD by adding PTFE, (b) specific capacitance vs. loading weight *[97]*.

Manganese oxide coatings for supercapacitor applications were also produced by electrophoresis [98]. The experiment was carried out under DC electrical field at a constant voltage of 100 V for 20 minutes. Manganese oxide particles were dispersed in ethanol suspension by sonication and graphite electrodes were utilized.

- Solid Oxide Fuel Cells (SOFCs)

Solid oxide fuel cells (SOFCs) have played a crucial leading role in power generation. Many scientists believe that SOFCs can revolutionize the future of science and technology due to the cells clean operation and efficiency. As it can be understood from the name, the difference between a SOFC and a conventional fuel cell is that the first one

uses a solid ion conductive ceramic as the electrolyte, while the latter works with liquid electrolytes [99]. The electronic conductivity of the dense electrolyte of a SOFC at the working temperature of approximately 600 to 1000C should be low [100]. Generally, in SOFCs, the cathode is exposed to open air or oxygen and oxygen is reduced to an oxygen anion. Then the oxygen anions travel through the electrolyte to the anode where hydrogen molecules or hydrocarbons are oxidized at the operating temperatures [101]. Lanthanum strontium gallium magnesium oxides (LSGMs), Lanthanum strontium cobalt ferrites (LSCFs), yttria stabilized zirconia (YSZ) and ceria gadolinium oxides (CGOs) which have remarkable long-term stability and strong mechanical properties are the most popular materials for electrolyte, while lanthanum strontium manganite (LSM), Ni foil, Ni/ZrO_2 cermet, Ni/YSZ substrates are used as cathodes and anodes [102, 103]. There are several challenges in fabrication of SOFCs such as their high operating temperatures and high layer thickness [104]. There are two possible approaches to solve these issues. First, as the operating temperature is completely dependent on the nature of the electrolyte material, there is always a possibility to find better materials with higher ion conductivity at lowered temperatures (500-800 ˚C) [105]. Second, it is known that reducing the thickness of the film can also lower the operating temperatures [106]. EPD has been widely exploited to fabricate SOFCs in the last two decades [107, 108, 109, 110, 111]. EPD is able to fabricate complex shapes, prepare both dense and porous films, and allows co-deposition of different source materials. Figure 9 shows the SEM images of the surface and the cross-section of a positive-electrolyte-negative cell [112].

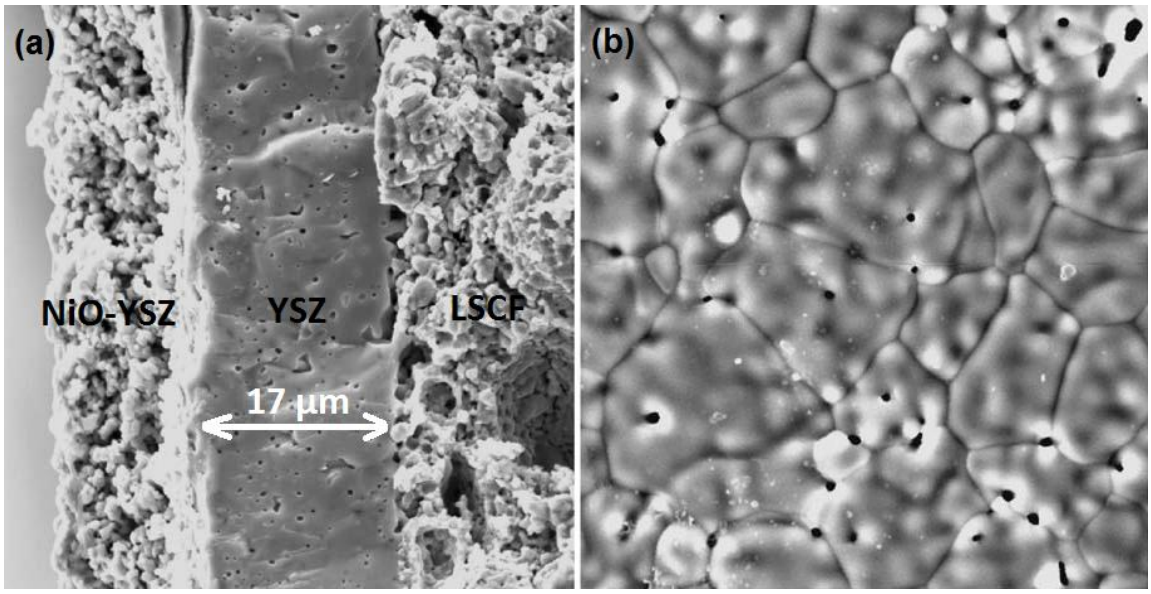

Figure 9 - SEM image of the sintered EPD films of positive-electrolyte-negative (NiO–YSZ/YSZ/LSCF) in a SOFC; (a) cross-section and (b) surface *[112]*.

Preparation of YSZ on LSM and LSM/YSZ substrates through EPD was carried out by a constant-voltage method [113]. Another research group successfully produced well-distributed LSGM films with good adhesion to platinum substrate from a suspension in a mixture of acetone and ethanol [114]. The right selection of solvent, dispersant and binder is of great importance in electrophoresis of ceramic laminates to be used in SOFCs. In one experiment, they found the best properties using ternary selection of ethyl alcohol, phosphate ester and polyvinyl butyral as solvent, dispersant and binder, respectively [115].

- Corrosion-resistant Coatings

EPD is one of the most promising techniques for fabricating thick-films, which may be applied to increase the corrosion resistance of metals. Corrosion-resistant coatings have been used for protecting different substrates that suffer from weak corrosion resistance [116, 117, 118]. Silica hybrid coatings have provided both excellent mechanical and corrosion resistance properties, they have drawn much attention in the last decade and EPD was commonly used to make corrosion protective coatings [119, 120, 121, 122]. One study compared corrosion behavior of silica hybrid coatings made by dipping with these made by EPD [123]. Stainless steel and graphite electrodes were used as the substrate and counter-electrode, respectively. Temperature was maintained at 5˚C during the whole procedure. EPD coatings were thicker than dipped coatings and had more enhanced corrosion resistance.

- Catalyst support and molecular sieves

Porous ceramics are used as catalyst supports and molecular sieves due to their corrosion resistance and high-temperature stability. In order to broaden and modify the range of their application, coatings are applied all over the outer and inner surface of these ceramics. Pore size and surface functionality must be controlled too in order to improve their properties. EPD makes possible embedding strong and uniform coatings on complex-shaped materials [124, 125], such as coating the inner surface of porous foams and tubes. Near-200 micron layer of alumina particles was deposited onto the inner surface of porous alumina tube via electrophoresis at a constant voltage of 100 V under

DC electrical field, using polypyrrole-coated glass and stainless steel as the substrate and the counter electrode, respectively [126]. Figure 10 shows SEM images of the inner wall of the non-coated and Ppy-coated tubes.

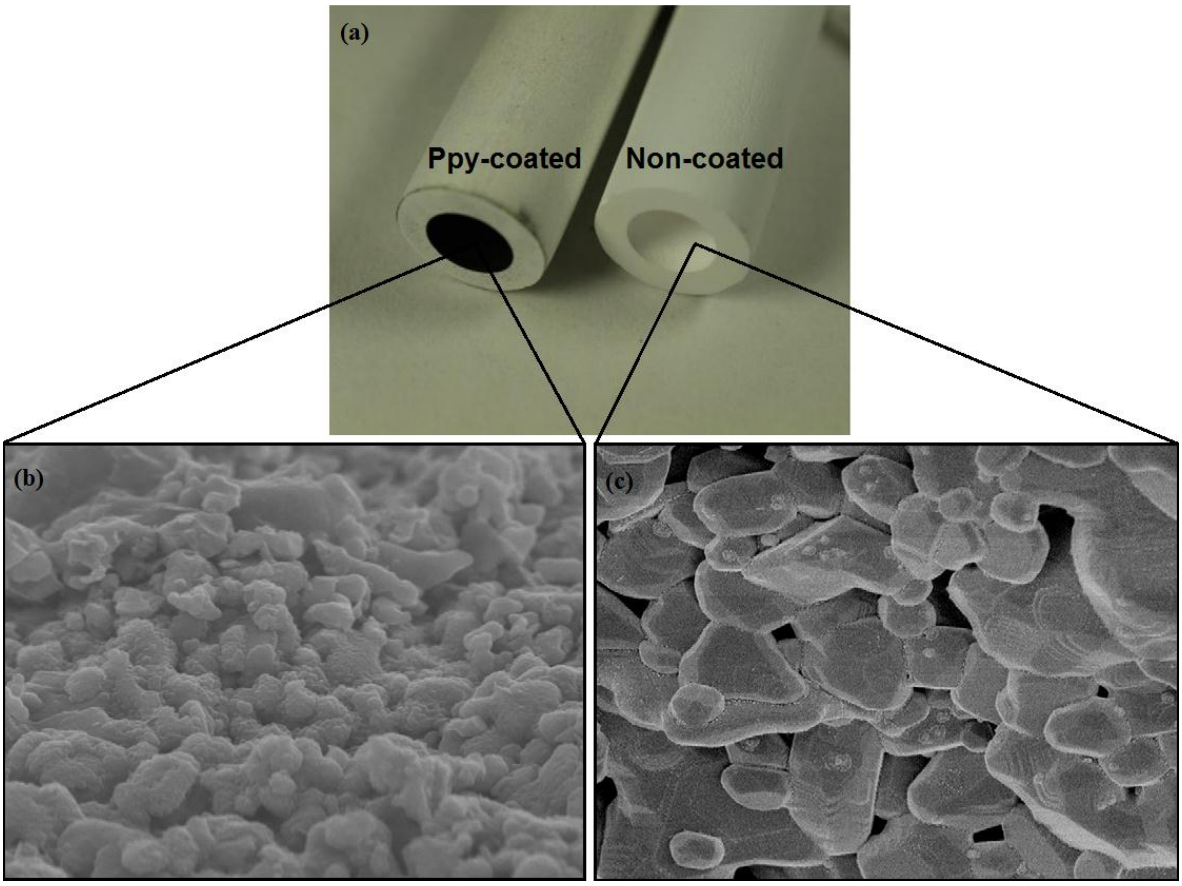

Figure 10 - (a) Porous alumina tubes and SEM images of the inner wall of (b) Ppy-coated and (c) non-coated tubes *[126]*.

- Sensors

Gas sensors, with high sensitivity, capability of real-time detection and economic efficiency, are widely used in industry [127]. EPD has greatly contributed in generating

both new original and modified production routes for production of common gas sensor films [128]. Figure 11 depicts a schematic sketch of the process of fabricating a gas sensor with anodic aluminum oxide (AAO)/Al substrate and SEM image of gas sensors fabricated with a current density of 90mAcm^{-2}. It is noteworthy that an insulator support has to be used between the gas sensing film and the conductive substrate, in order to avoid of a short circuiting between these two layers [129].

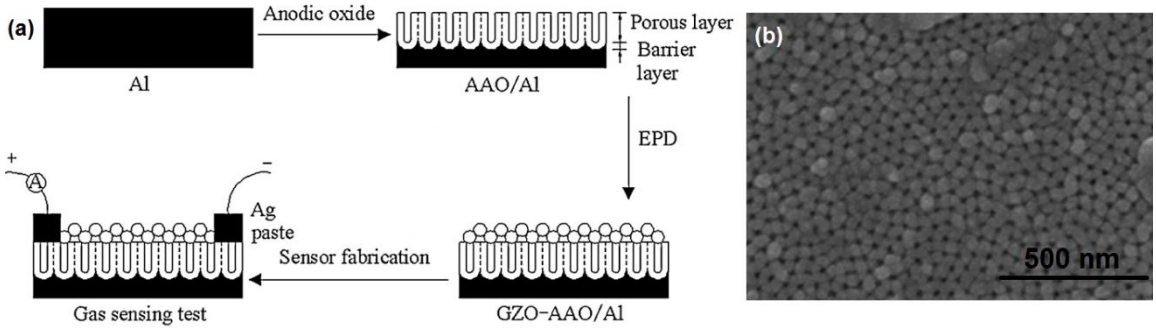

Figure 11 - Schematic sketch of fabricating gas sensor via EPD *[130]*.

Al-Cr-Fe conductive substrate was electrophoretically coated by zinc oxide in construction of one of the sensors [131]. Another sensor was constructed using aqueous EPD of aluminum oxide on aluminum substrate [130].

- Piezoelectric actuators

Piezoelectric actuators (Pas) use voltage induced size changes of ferroelectrics for highly-accurate mechanical actuators. A good PA provides high forces at low voltages. In addition, low sintering temperature and high Curie temperature and high piezoelectric constant are very importatnt [132, 133]. Pas are utilized in a wide range of applications, from optical to aerospace industries [134, 135, 136]. Pas suffer from weak mechanical

properties at both low and high temperatures and their efficiency is highly dependent on the continuity and uniformity of their structures. EPD has been proven to successfully solve these shortcomings due to its intrinsic properties. Two versions of piezoelectric actuators based on Pb-Zr-Ti-Bi-Fe-Ba-Cu-W oxides (PZT1 and PZT in Fig17) were tested in functionally graded structures with silver coated electrodes (Figure 12) [137]. The results confirmed formation of a piezoelectric actuator.

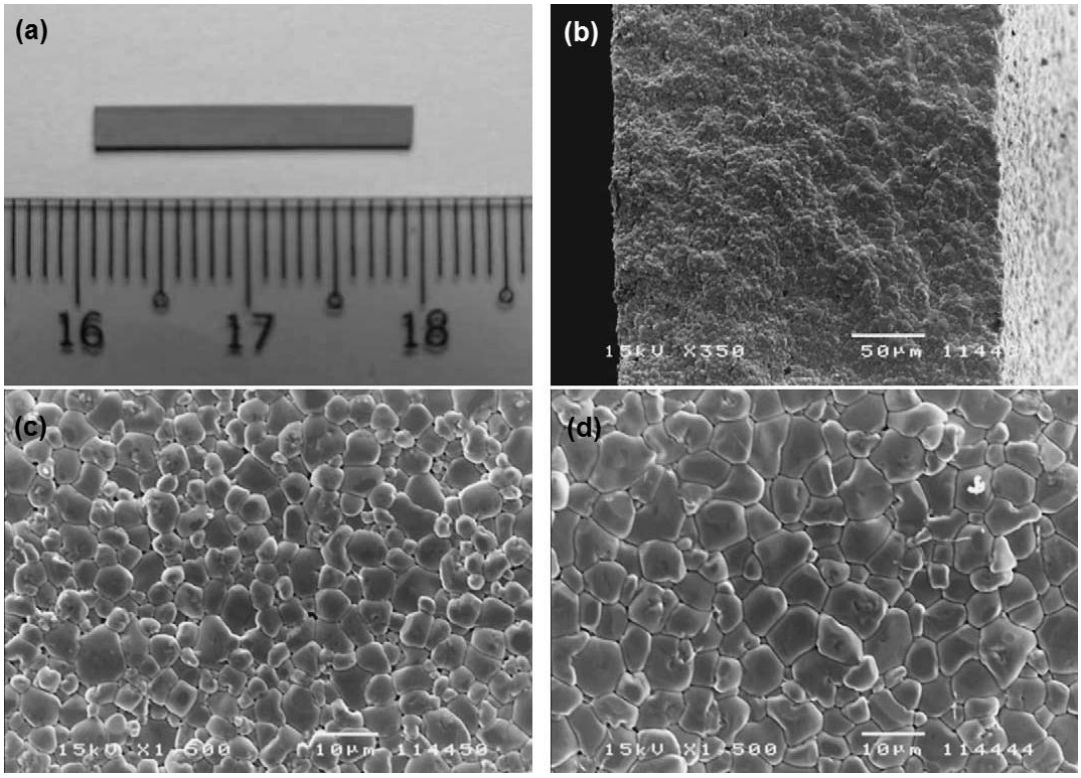

Figure 12 - Microstructure of piezoelectric functionally graded monomorph actuator; (a) plate, (b) cross-section, (c) PZT surface, and (d) PZT1 surface *[137]*.

In another investigation, EPD was used to deposit piezoelectric layer on a graphite rod from a suspension containing doped piezoelectric material (Figure 13) [138].The

graphite rods were removed from the spiral shape, resulting in complex-shape PA actuators that would be very difficult to make using traditional methods. The studies showed that EPD is a promising method in production of PAs.

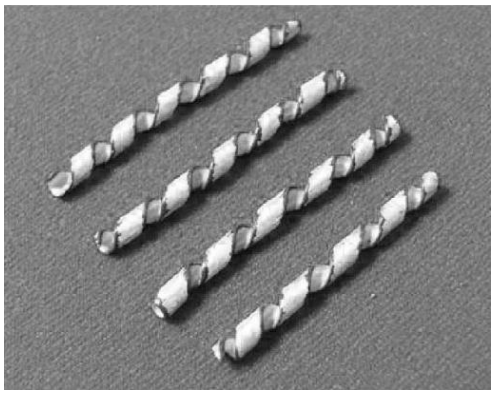

Figure 13 - Image of piezoelectric actuators made by deposition on graphite rods *[138]*.

- Forming biocompatible layers

In general, metallic biomaterials which are widely used as prosthesis and implants have one important shortcoming which is their bio-inert nature [139]. Overcoming this problem, EPD can form bioactive ceramic coatings [140]. Amongst all, electrophoresis of hydroxyapatite (HA) and bioactive glass (BG) has been vastly investigated by scientists [141, 142, 143, 144, 145].

HA ($Ca_{10}(PO_4)_6(OH)_2$) is a crystalline mineral that has very similar chemical composition to bone and teeth tissue and as it has excellent biocompatibility, osteoconductivity and bioactivity; it is widely used as hip replacements and dental implants [146, 147, 148, 149]. Processing HA via a powder route has many difficulties, for example, sintering must be done at relatively high temperatures, which may sacrifice

the biocompatibility and decompose the favorable HA structure [150]. It was demonstrated that electrophoresis of thermal-sprayed HA powders in ethanol suspension at a pH of 5, using graphite and stainless steel electrodes, leads to successful preparation of porous hydroxyapatite scaffold (Figure 14-a) [151]. In comparison to salt leaching and microsphere burn out, which are two popular routes for fabrication of porous scaffolds, EPD has the advantages of needing no additives or binders and being a simpler process, although the costs of preparing large components are higher. As HA has poor mechanical properties, its applications are mostly in coating and composites with metallic substrates and matrices. Deposition of submicron HA in the form of a thick coating by EPD has been reported (Figure 14-b) [152]. Ethanol suspension and ultrasonic agitation was used in order to disperse the thermal-plasma-sprayed HA particles. EPD process was carried out at pH value of 3-5 and under current density of 0.05-1.5 mA/cm^2 for 90 seconds. Carbon rod and stainless steel cylinder were used as the substrate and the counterelectrode, respectively. Recently, another group has studied the formation of HA nanocomposite coatings in alcohols [153]. In their investigation, two 316L stainless steel plates were used as electrodes and the experiment was carried out at voltages of 20 and 60 V/cm for up to 10 minutes. The quality of HA-chitosan nanocomposites were tested in alcoholic suspensions using methanol, ethanol and isopropanol. Results revealed that the adsorption of chitosan on HA nanoparticles showed its highest and lowest levels, in isopropanol and methanol, respectively.

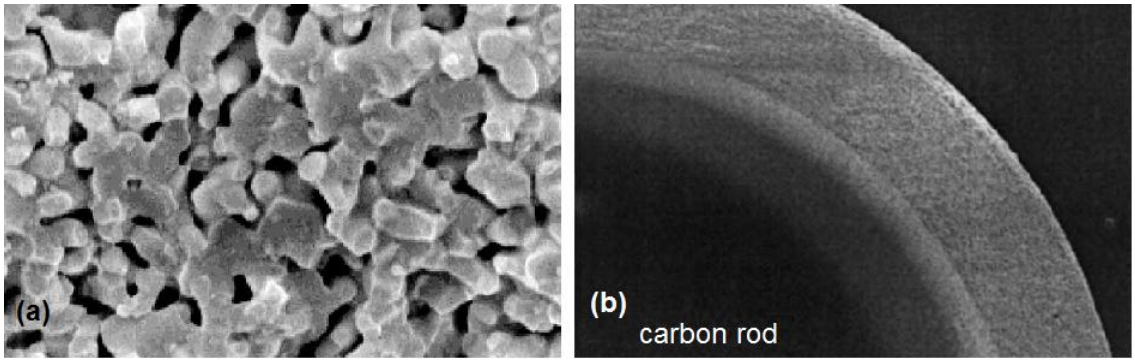

Figure 14 - (a) Interconnectivity of porous HA scaffold fabricated, (b) dense, uniform and crack-free HA tube both prepared by EPD *[152, 78]*.

BG (FDA approved composition of a mixture of SiO_2, CaO, Na_2O and P_2O_5) is a surface reactive glass biomaterial with a very good biocompatibility [154]. The deficiencies of both BG and some metallic implants (which are low corrosion resistance and low biocompatibility [155]) were eliminated by coating BG on the metallic implants. Figure 15 shows deposited BG composite on Ti wire. In one study, BG was electrophoretically deposited on 316L stainless steel substrate in a mixture of ethanol and triethanolamine as the suspension at constant voltages of 30, 60 and 90 V/cm^2. They have also reported that the layer acts as a barrier layer in artificial saliva [156]. In another study, EPD of BG/polymer composite coatings were made at a constant voltage range of 10-30 V and pH level of 11 [157].

Moreover, EPD has helped to develop novel bioactive composites. For example, wollastonite ($CaSiO_3$) particles were deposited into porous alumina and porous ultrahigh molecular weight polyethylene in a suspension of iodine and acetone at a constant

voltage of 1000 V for 60 minutes. In the procedure, accumulation of wollastonite particles occurred near the cathode surface [158].

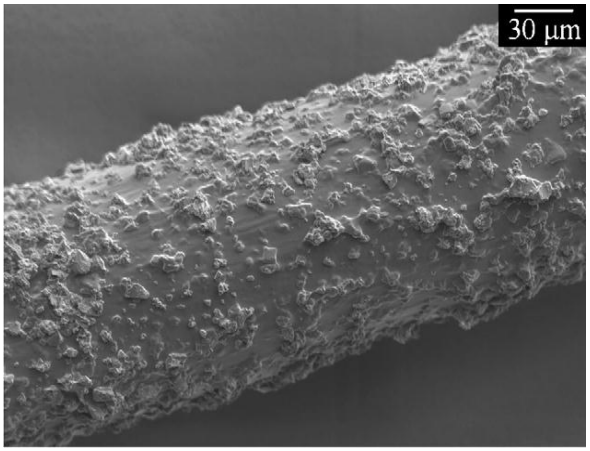

Figure 15 - Alginate/BG composite deposited on Ti wire *[157]*.

- EPD of bacteria

In addition, EPD of bacterial cells was carried out and the interesting results of the investigation have opened new windows to electrophoresis of inorganic materials [159]. In that investigation, a mixture of demineralized water and sucrose ($C_{12}H_{22}O_{11}$) was used as. The experiment was done under AC field at a constant voltage of 100 V and a frequency of 25 Hz for 10 minutes. Confocal laser scanning microscope image (Figure 16) demonstrated that both live Gram-positive and Gram-negative bacteria were successfully deposited; however, the viability of the bacteria cells was compromised after the deposition.

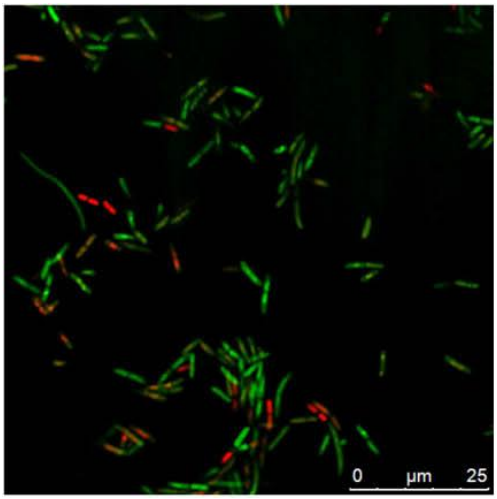

Figure 16 - Confocal laser scanning microscope image of electrophoretically deposited bacteria after 2400 s *[159]*.

- Corrosion protection of implants

Magnesium alloys have an outstanding strength to weight ratio, suitable biodegradability and non-toxicity which make them appropriate candidates for implants. The major drawback for these alloys is their low corrosion resistance in the body. EPD has been shown to be useful in forming corrosion resistant coatings on magnesium bio implants [160]. AZ91 Mg alloy bio-implants were coated by nanostructured akermanite ($Ca_2MgSi_2O_7$) to improve the corrosion resistance of these implants. Akermanite nano powders were suspended and then ultrasonically dispersed in methanol and immediately deposited electrophoretically on micro arc oxidized (MAOed) AZ91 Mg alloy substrates. EPD process was carried out at constant voltage of 100 V for 3 min. The resulting samples were then immersed in simulated body fluid (SBF) to study the corrosion rate. Figure 17-a shows SEM morphology of AZ91 after MAO and coating with akermanite;

Figure 17-b demonstrates the comparative results of the immersion test for studying the corrosion behavior of AZ91 before and after being assisted by MAO and coating. As can be seen, the corrosion rate has been significantly reduced after applying MAO and akermanite coating. It is noteworthy that the porous coating has been made intentionally in order to enhance biological fixations of the living tissue to the implant.

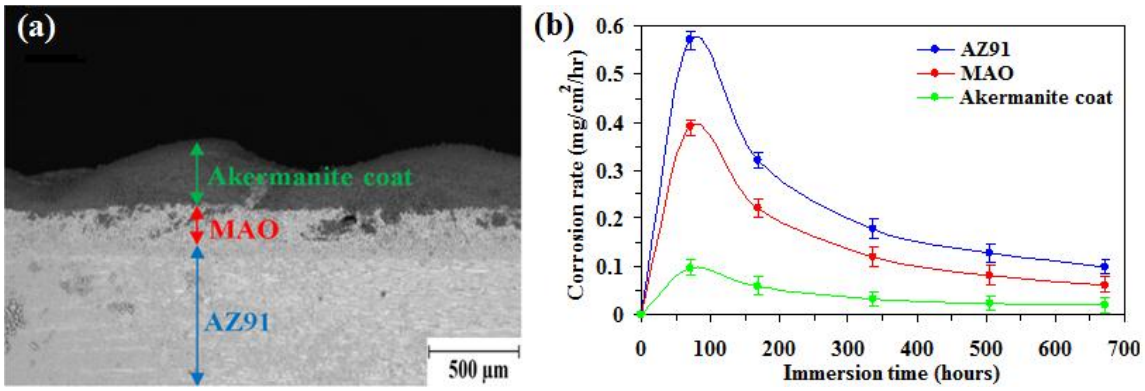

Figure 17 - (a) Cross-section view of the SEM morphology of final sample. (b) Corrosion rate of AZ91, MAO and akermanite coated samples immersed in SBF *[160]*.

1.3.4. EPD for thermoelectric thin/thick-films

EPD has shown great capabilities in making films with thicknesses from sub-micron to hundreds of micron, while maintaining the composition of the starting materials with stoichiometric ratios. In that project [29], our group prepared $Si_{80}Ge_{20}$ powder via milling and then sonicated the resulting material in acetone for 2 h in order to avoid any agglomeration and achieve a homogeneously dispersed colloidal solution. Silicon wafer was used as the substrate and it was etched in buffered oxide etch solution for 2 min, and

then washed with deionized water to remove the native SiO_2. The process was carried out in a custom-made cell under a constant voltage of 30 V at room temperature. After that, the sample was dried at room temperature and then cold pressed under 30 MPa pressure. Afterward, the coated substrate was sintered for 3 h at 1200˚C in nitrogen atmosphere. Figure 18 shows a SEM image and a photograph of $Si_{80}Ge_{20}$ layered on silicon substrate. Formation of dense and uniform layers of $Si_{80}Ge_{20}$ can be seen in Figure 18-a, while Figure 18-b shows the overall uniformity of the thick-films. Seebeck coefficient and electrical conductivity measurements from the room temperature to 950 ˚C showed that the TE power factor of $Si_{80}Ge_{20}$ thick-film is approximately $1.9 \times 10^{-3}\ \mathrm{W.m^{-1}.K^{-2}}$, which is an order of magnitude larger than the previously achieved values for thin-films of this material.

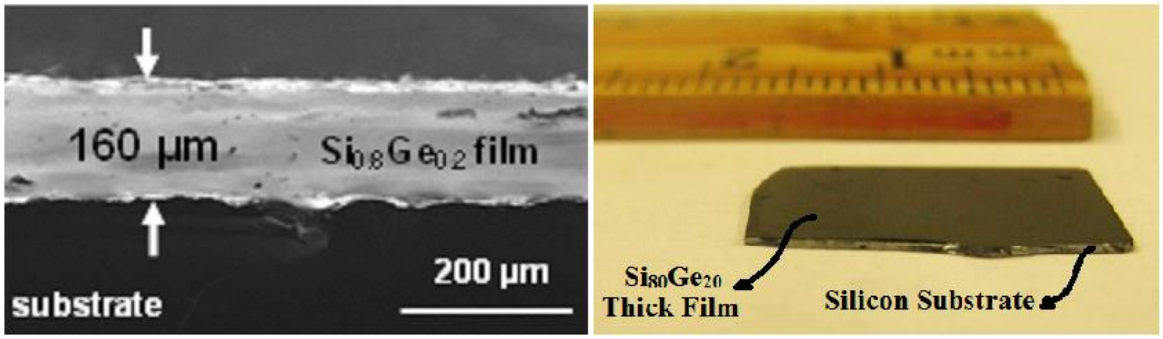

Figure 18 - (a) SEM image and (b) photograph of $Si_{80}Ge_{20}$ EPD coating sintered on silicon substrate *[29]*.

To date, there are only a limited number of studies available [28]. In this investigation, TE properties of electrophoretically deposited SiGe/Glass thick-films on two different substrates have been studied.

CHAPTER 2

Aims and Objectives

The objectives of this thesis were to develop a new method for growing thin film TE materials which is cost effective and allows material growth with thickness and roughness appropriate for making efficient TE devices.

The first aim of this project was to deposit a TE thick-film with thickness more than 100 μm.

The second aim was to reduce the surface roughness of the deposited film by 5% of its thickness.

The third aim was to characterize the TE properties of the deposited films and to estimate their TE figure-of-merit, ZT.

CHAPTER 3

Materials and Methods

3.1.Materials preparation

In order to synthesize Boron-doped $Si_{80}Ge_{20}$/Glass composite powder, stoichiometric ratios of Silicon (Si) and Germanium (Ge) powders were mixed along with 1.2 wt. % Boron (B) via mechanical ball milling. Ball milling was carried out at ambient temperature in a high-energy planetary ball mill (Fritsch, PULVERISETTE 7), via tungsten carbide vial and balls for 5h at ball to powder ratio and rotational speed of 20:1 and 950 rpm, respectively. To prevent the temperature rise, an interval of 3 min was applied for every 7 min milling. Powder samples were sealed and then annealed in a muffle furnace at 1100 °C for 3 h under Argon atmosphere. Then, 10 wt. % of Glass powder was milled along with the annealed powder for 5 h by the aforementioned ball milling conditions to make $Si_{80}Ge_{20}$/Glass composite powder.

3.2.EPD setup

1 gram of the prepared powder was sonicated in 150 mL of acetone for 1 h and afterwards was magnetically stirred for 15 min. Figure 19 shows the custom-made EPD setup used for these experiments. The non-conductive polymeric cap that has a circular window in it, sits on the electrode with the substrate in order to control the area that is being deposited under the electric field.

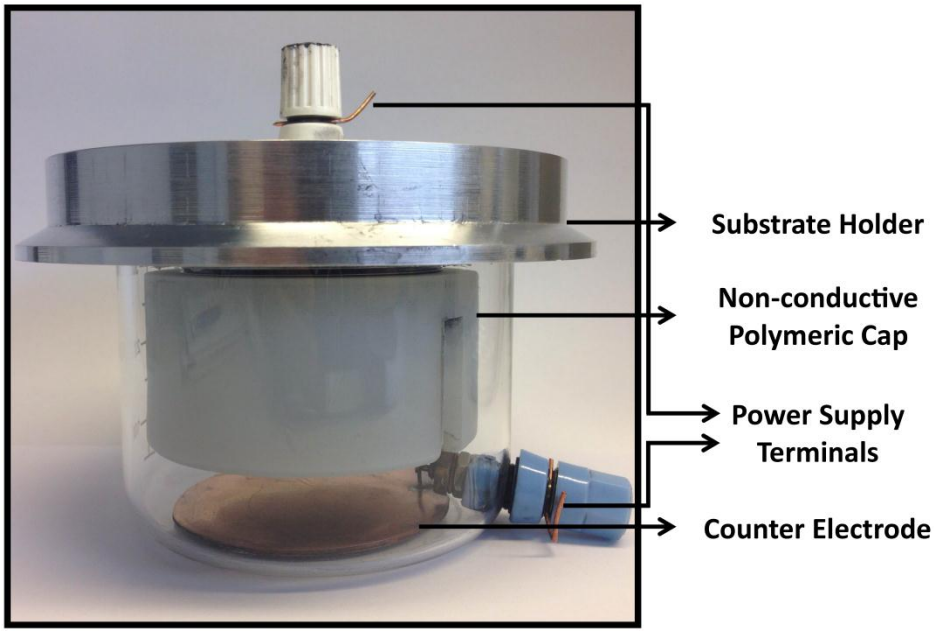

Figure 19 - Custom-made EPD setup.

The EPD process was performed using a DC power supply (HY3010E Mastech Co) and in a custom-made setup. Two different sets of substrates were used in our investigations. In the first sets of experiments, silicon substrate was gently scratched by sand paper, and etched in HF solution for 2 minutes and finally washed with deionized water to remove probable native silicone oxide from the surface of silicon substrate. In the second sets of experiments, 2 inch diameter, double side polish *(0001)* sapphire discs (Saint-Gobain) have been used as the substrates. Sapphire is electrically non-conductive but it has the virtue of good IR transmittance. In order to make the substrates conductive, one side of the sapphire discs have been first roughened by polishing and then coated with pure chromium via a sputtering system (ATC Orion: AJA International, Inc.) in a class 100 clean-room facility. Chromium has good IR absorption, which makes it a good

candidate for absorbing the 1064 nm IR Laser waves for measuring the thermal conductivity.

Putting the prepared substrates and a circular copper plate with a 20 mm distance as the cathode and anode, respectively, the process was carried out at a constant voltage of 500 V for 5 min. After extracting the substrates carefully drying them at room temperature, the next step, which was sintering, was done at 1300 °C for 5 h at a heating rate of 2 °C/min.

3.3.Characterization

In case of microstructural studies, the X-ray diffraction (XRD: Bruker D8 Discover system operating with 0.8 mm beam size at a generator voltage of 40 kV, tube current of 40 mA and Cu-Kα radiation) and scanning electron microscope (SEM: Hitachi S-4800) were utilized. Surface topography and roughness analysis of the as-deposited and as-sintered films has been studied through a laser scanning electron microscopy (Keyence, VK X100/X200) via using three dimensional images.

3.4.Thermoelectric measurements

Seebeck coefficient (S) and electrical conductivity (σ) of samples were measured with four probe method from room temperature to 950 °C by means of commercially available equipment (ULVAC, ZEM-3). Furthermore, the thermal diffusivity (α) was measured the

samples via a laser flash apparatus (Netzsch, LFA 457). The thermal conductivity (κ) was then calculated from equation (3),

$$\kappa = \rho C_P \alpha \tag{3}$$

where ρ is the bulk density of the sample and C_P is the specific heat. For determining the specific heat of the samples, C_P was simultaneously measured and compared with a Pyroceram (reference sample which had results in good agreement with the literature data) [161]. At last, TE figure-of-merit (*ZT*) was calculated through equation (1).

CHAPTER 4

Results and Discussions

4.1.Thick-film on Si wafer structural characterization

Figure 20 shows XRD plots of as-milled, as-deposited and as-sintered SiGe/glass powder (a), and SEM photomicrographs of as-milled (b, c), as-deposited (d, e), and as-sintered (f, g) SiGe/glass powder on the silicon substrate in different magnifications. XRD patterns indicated only three peaks at $2\theta = 28.37^{\circ}$, 47.16° and 56.04° corresponding to SiGe. Because glass has an amorphous structure, it does not have any contributions to the diffraction pattern. So typically, for $Si_{80}Ge_{20}$/Glass composite XRD pattern, what we see is the peaks for pure silicon but with a slight shift caused by alloying with germanium.

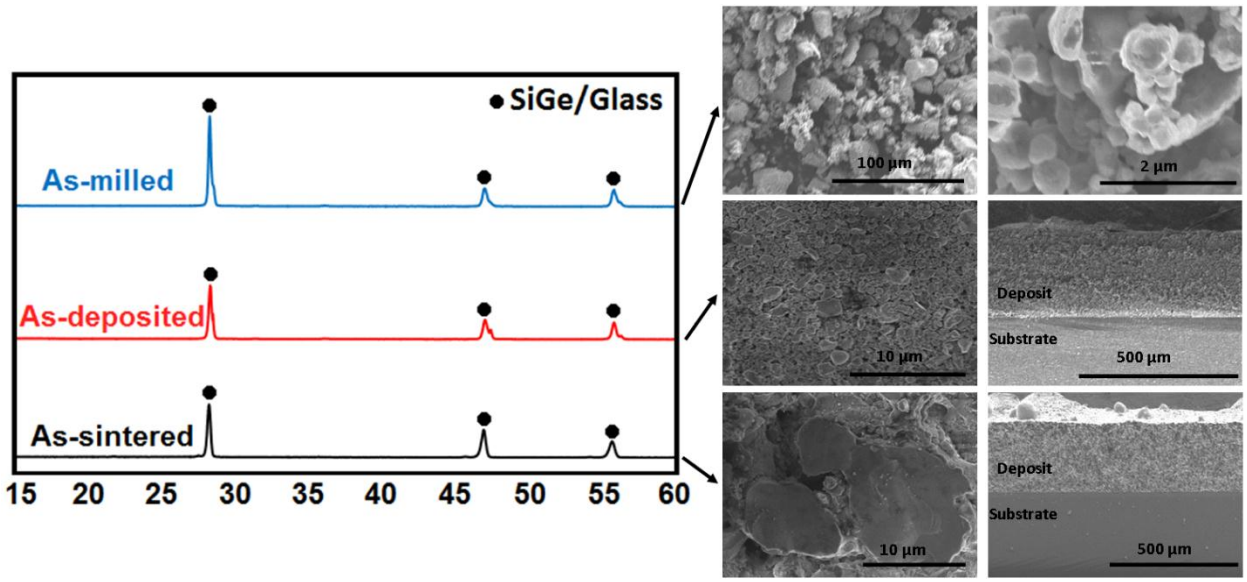

Figure 20 - (a) XRD patterns of the as-milled, as-deposited and as-sintered samples and SEM images of (b, c) as-milled powder, (d, e) as-deposited sample and (f, g) as-sintered sample.

Figure 21 shows the SEM photomicrograph of cross-sectional view of as-deposited SiGe/glass powder on the Si substrate. This Figure indicates the distribution of both particles and porosities with different sizes during the EPD process. As can be observed in the Figure, at the first stage of EPD process, the fine particles have moved to deposited on the surface. In next layers, the size of particles has increased gradually with the increasing the distance from the substrate and they exhibiting granular morphology. It may be due to the presence of particles with various sizes in the EPD solution. The small particles being consumed and move faster than bigger particles by applying a specific voltage inducing the distribution profile of particles on the substrate surface. Moreover,

the size and amount of porosities enhanced from the surface until the top of the deposited film as can be seen in Figure 21. Because by increasing the particle sizes the distance between the particle boundaries enhances leading to the existence of more porosities.

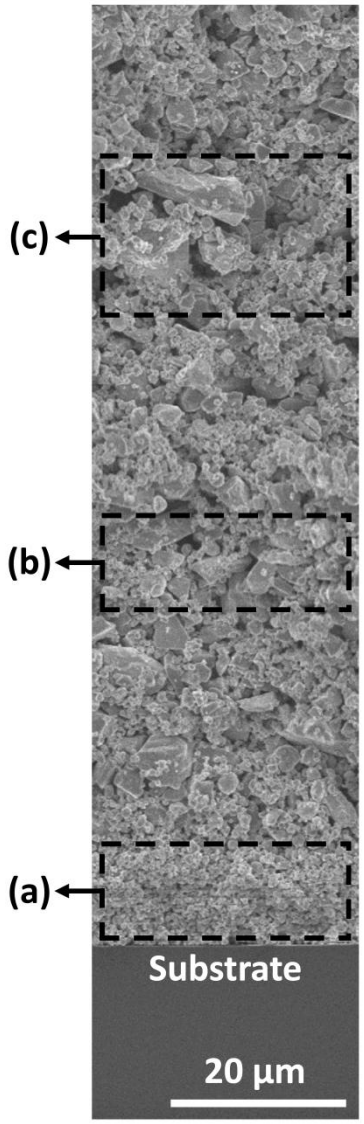

Figure 21 - Cross-sectional SEM image of the as-deposited sample; regions (a) close, (b) mid-far and (c) far relative to the substrate.

4.2.Thick-film on Si wafer thermoelectric measurements

Figure 22 shows the experimental data of the thermal conductivity from room temperature to 800 °C. The results show that the thermal conductivity is a function of temperature, whereas it decreased from room temperature until 470 °C, and increased again until the 800 °C. The thermal conductivity decreased from 3.54 W/Mk to 3.1 W/Mk in the specific range of room temperature to 470 °C, and then increased from 3.1 W/Mk to 3.3 W/Mk during the 470 °C to 800 C. Thus, the best thermal conductivity occurred in 470 °C according to our results.

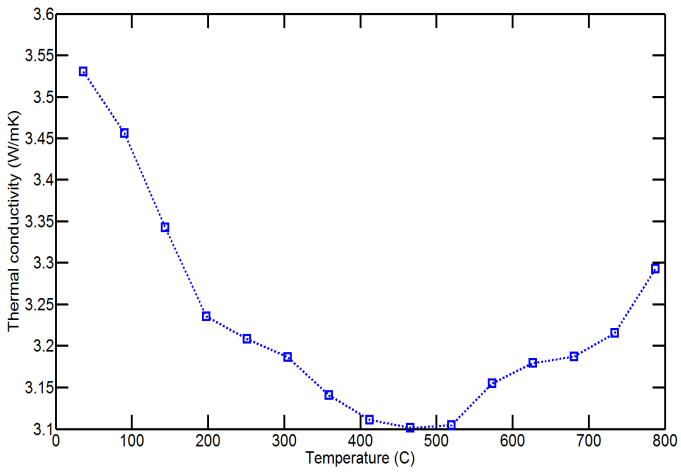

Figure 22 - Temperature dependence of thermal conductivity of the sample on Si wafer.

Figure 23 shows the experimental data of (a) electrical conductivity, (b) Seebeck coefficient, (c) power factor times temperature and (d) TE Figure-of-merit, ZT versus temperature from room temperature to 800 °C. The electrical conductivity (Figure 23-a) shows an approximately constant value of about 13 S/cm in the range of 400-650 °C, with a significant increase up to 22.5 S/cm between 650 to 800 °C. The constant behavior

of electrical conductivity (400-600 °C) may be due to the non-degenerate carrier concentration. The Seebeck coefficient has been indicated a similar trend to electrical conductivity as shown in Figure 23-b indicating the dependence of Seebeck coefficient of deposited film to electrical conductivity. The Seebeck coefficient increased with increasing electrical conductivity which may be due to increasing carrier concentration. The temperature dependence of power factor according to Figure 23-c showed that the TE power factor of produced thick-film is about 0.025 W/mK above 450 °C. Theoretical modeling of charge transport has showed that the enhancement of the power factor is due to the high carrier mobility of the film, which is in accordance with their dense and uniform structure. Figure 23-d shows the TE figure-of-merit (ZT) as a function of operating temperature. According to this figure, the sample shows the highest performance near 450-500 °C temperature. Moreover the observed reduce in thermal conductivity between 450-600 °C due to phonon scattering helps to enhancement of ZT. The concentration of the holes increases with temperature and becomes comparable to that of the electrons at about 450 °C, which is responsible for the increment of the electrical conductivity and the Seebeck coefficient above this temperature.

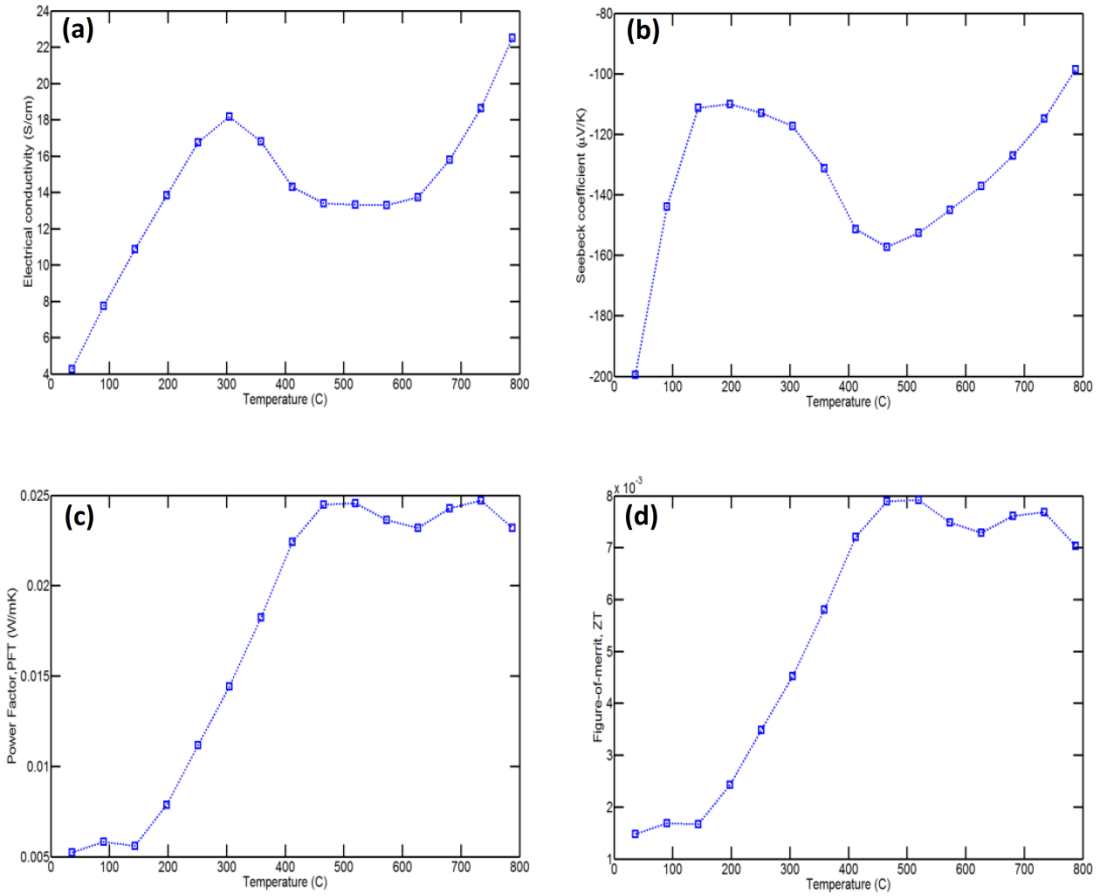

Figure 23 - (a) Electrical conductivity, (b) Seebeck coefficient, (c) power factor times temperature and (d) TE figure-of-merit ZT of thick-films on Si wafer.

The fact that the electrical conductivity is smaller than the typical values for bulk $Si_{80}Ge_{20}$ TE alloys attribute to the lower electron concentration or the lower electron mobility due to the carrier scattering by crystal defects in the film. However, the Seebeck coefficient decreased with temperature, which indicates that the increase in the carrier concentration with temperature is the dominant effect.

Poor electrical properties of this sample are due to the loss dopants during the sintering process (diffusing to the Si substrate) and its porous structure.

4.3.Boron diffusion into un-doped Si wafer

Assuming the appropriate initial conditions, boron diffusion profile can be theoretically calculated. Based on SILVACO models that studied the complex couplings between boron and point defects on diffusion with a constant surface concentration [225], when the initial concentrations to be equal to 10^{20} cm^{-3}, raising the temperature up to 1300 ˚C for 3 h leads to diffusion of boron atoms to the depth of 23 μm. Given the fact that there is huge difference between the resistivity of the un-doped section and the section with dopants, the theoretical value was also confirmed after polishing off the substrate and measuring the resistivity.

4.4.Thick-film on Sapphire substrate structural characterization

Surface topography and roughness of both as-deposited and as-sintered films are presented in Figure 24. All of the following images have been processed by the VK software and the results are root mean square values from various parts of the sample. Figure 24-a, shows a two dimensional (2D) electron microscopy analysis of the as-deposited sample. According to the inset which is the overall line-scan profilometry, average roughness of the as-deposited film is 10 μm. According to the profilometry measurements for the as-sintered sample, that is given in the inset of Figure 24-c, the

average roughness has reduced to 5 µm which can be justified by reduction of porosities due to sintering. A comparison between the three dimensional (3D) demonstrations of the as-deposited and as-sintered samples which are provided in Figure 24-b and Figure 24-d, respectively, confirms that the roughness of $Si_{80}Ge_{20}$/Glass composite thick-films has reduced after sintering. As it can be seen, the area of the red islands with roughness of 10 µm has reduced to a great extent and the 3D electron image of the as-sintered sample (Figure 24-d) seems to be smoother, less rough and more uniform.

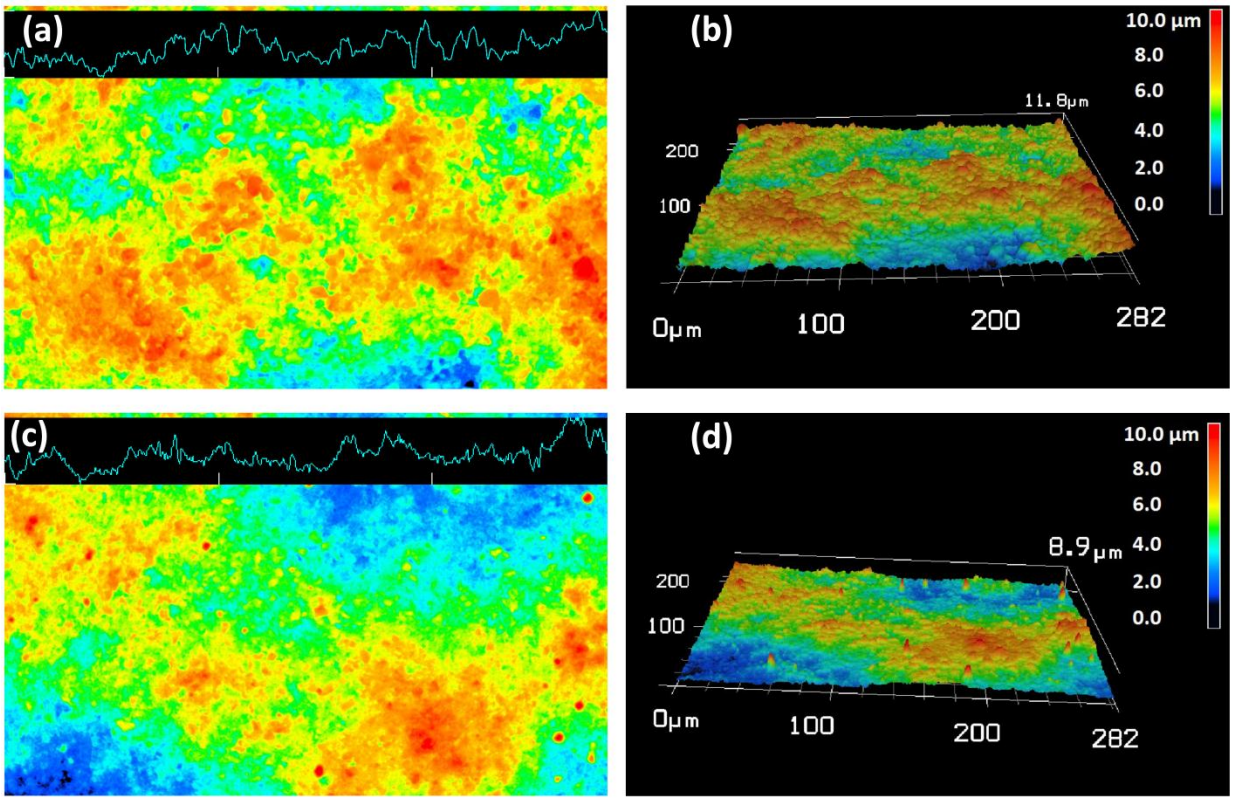

Figure 24 - Surface topography and roughness of: (a) as-deposited (2D), (b) as-deposited (3D), (c) as-sintered (2D) and (d) as-sintered (3D) $Si_{80}Ge_{20}$/Glass composite thick-films.

Figure 25 shows the SEM images of the as-sintered $Si_{80}Ge_{20}$/Glass composite thick-films. The top view image, Figure 25-a, shows that the neighboring particles have diffused in each other and necked which is the signature of sintering powder particles. Also, it can be seen that although the porosity has reduced after sintering, the fabricated thick-film still has some porosities which will definitely sacrifice the electrical properties. The thickness of the film, that has been given in the cross-sectional view in Figure 25-b, has been calculated to be equal to 725 µm.

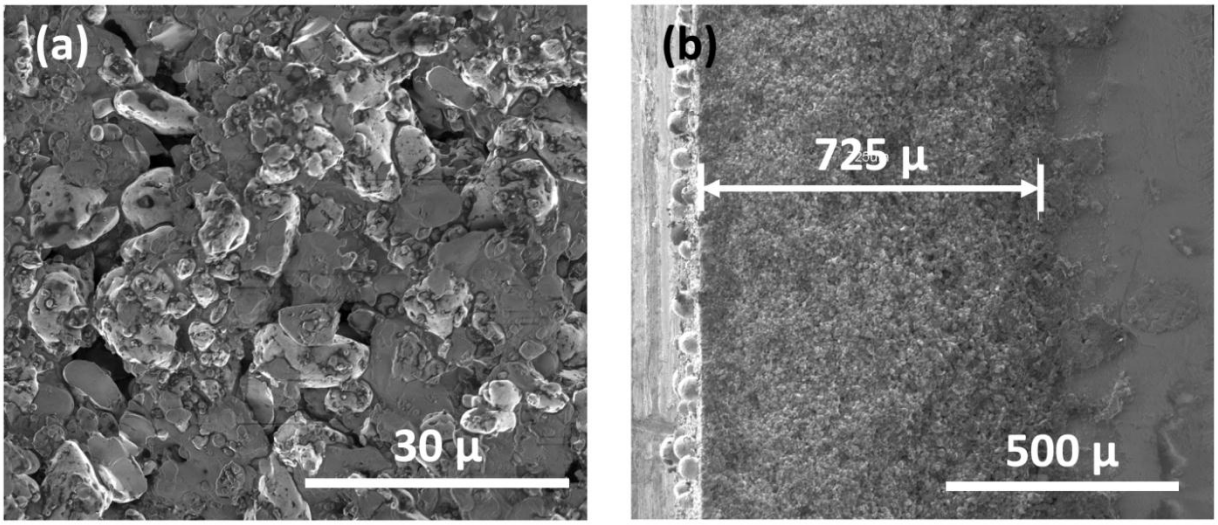

Figure 25 - SEM (a) top-view and (b) cross-sectional view image of the as-sintered $Si_{80}Ge_{20}$/Glass composite thick-film.

4.5.Thick-film on Sapphire substrate thermoelectric properties

Temperature dependence of the electrical conductivity (σ), Seebeck coefficient (S), power factor times temperature (PFT), thermal conductivity (K) and the dimensionless TE figure-of-merit (*ZT*) have been presented in Figure 26. The temperature range is from room temperature to 900 ˚C. It can be seen that the value of electrical conductivity, which is less than the bulk SiGe values due to porosity, decreases by increasing the temperature which can be justified by the reduction of carrier mobility due to the increase in electron-acoustic phonon scattering at high temperature. After 850 ˚C, the enhancement of intrinsic conduction compensates for the electrical conductivity and its reduction stops. The Seebeck coefficient measurements show an inverse proportion to electrical conductivity values. This room temperature value for the Seebeck coefficient confirms that the prepared thick-film is highly doped and the hole concentration is relatively high. The amount of active boron concentration is highly dependent on the processing and synthesis parameters which have been previously optimized [162]. In Figure 26-c the temperature dependence of power factor times temperature is demonstrated. The calculated values are approximately an order of magnitude higher than the previously reported values for SiGe thin-films [29]. Studying the thermal conductivity values for the prepared thick-film illustrates that although its values reduces at some points, the overall trend shows an increase in thermal conductivity by increasing the temperature. Increase of phonon–phonon scattering reduces the thermal conductivity [163], while increasing the ambipolar thermal conduction results in elevating the thermal conductivity values

[164]. Overall, the thermal conductivity values are small because of the porous structure of the films. At last, the temperature dependence of TE figure-of-merit ZT of the prepared $Si_{80}Ge_{20}$/Glass composite thick-film is presented in Figure 26-e. The high temperature value of ZT equal to 0.2 is comparable to the ZT of *p*-type bulk crystalline $Si_{80}Ge_{20}$ which is around 0.5 [162]. It is noteworthy that it is the first time to report the ZT value for thin/thick-films fabricated via EPD. This ZT can be improved by making the samples more dense which results in increasing the mobility.

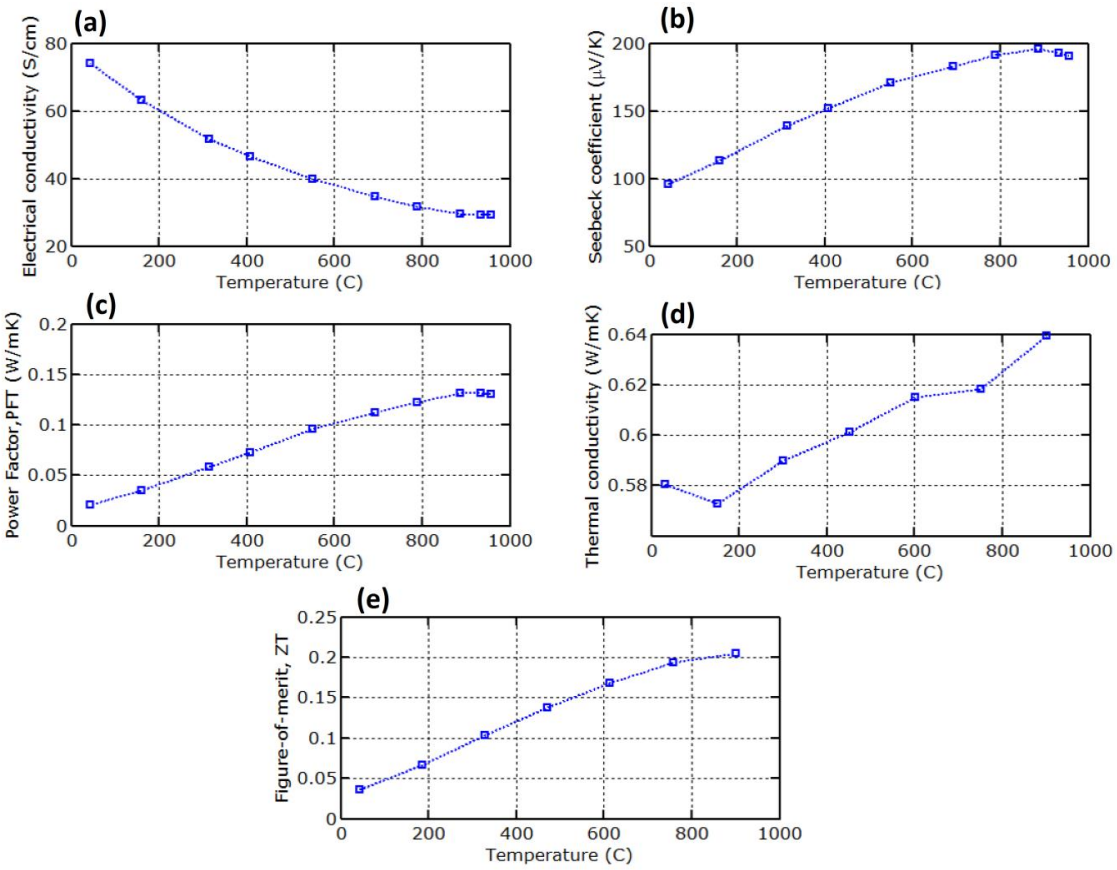

Figure 26 - (a) Electrical conductivity, (b) Seebeck coefficient, (c) power factor times temperature (d) thermal conductivity, and (e) TE figure-of-merit ZT of $Si_{80}Ge_{20}$/Glass composite thick-films.

CHAPTER 5

Conclusions

Boron-doped $Si_{80}Ge_{20}$/Glass composite films have been grown successfully on both Si wafer and Sapphire substrates and the temperature dependence of the electrical conductivity, Seebeck coefficient, power factor times temperature, thermal conductivity and the dimensionless TE figure-of-merit have been evaluated and, for the samples on Sapphire substrate, their high temperature values were approximately equal to 30 (S/cm), 200 (μV/K), 0.15 (W/mK), 0.64 (W/mK) and 0.2, respectively. It is the first time to report *ZT* for electrophoretically deposited TE thick-films and the *ZT* value is comparable to the present reported *p*-type SiGe bulk values. The samples on Si wafer had poor TE properties due to their loss of dopants during the sintering process.

CHAPTER 6

Future Directions

For the future research on the discussed topic, it is suggested that a better TE figure-of-merit, ZT can be achieved through reduction of porosities in the deposited films. For example, the sintering process, which in this project was carried out in a muffle furnace under controlled atmosphere, can be done via a hot press furnace. Pressing the film when it is being heated up to its sintering temperature can reduce the porosity of the final product to great extent; while resulting in a more smooth and shiny finish. The hot pressing can also reduce the sintering time from hours to minutes, which would be more appropriate for commercialization.

REFERENCES

[1] D. Andrews, Energy Harvesting Materials, New Jersey, United States: World Scientific Publishing Company, 2005.

[2] T. Tritt and M. Subramanian, "Thermoelectric Materials, Phenomena, and Applications: A Bird's Eye View," *Materials Research Society Bulletin,* vol. 31, no. 3, pp. 188-198, 2006.

[3] N. G.S., J. Sharp and H. Goldsmid, Thermoelectrics, Berlin, Germany: Springer, 2001.

[4] D. Rowe, CRC Handbook of Thermoelectrics, Florida, United States: CRC Press, 1995.

[5] X. Gou, H. Xiao and S. Yang, "Modeling, experimental study and optimization on low temperature waste heat thermoelectric generator system," *Applied Energy,* vol. 87, no. 10, pp. 3131-3136, 2010.

[6] R. Mahajan, C.-P. Chiu and G. Chrysler, "Cooling a microprocessor chip," *Proceedings of the IEEE,* vol. 94, no. 8, pp. 1476-1486, 2006.

[7] M. Elsheikh, D. Shnawah, M. Sabri, S. Said, M. Hassan, M. Bashir and M. Mohamad, "A review on thermoelectric renewable energy: Principle parameters that affect their performance," *Renewable and Sustainable Energy Reviews,* vol. 30, pp. 337-355, 2014.

[8] A. Loffe, Semiconductor thermoelements and thermoelectric cooling, London, United Kingdom: Infosearch, 1957.

[9] S. Bux, R. Blair, P. Gogna, H. Lee, G. Chen, M. Dresselhaus, R. Kaner and J. Fleurial, "Nanostructured bulk silicon as an effective thermoelectric material," *Advanced Functional Materials,* vol. 19, pp. 2445-2452, 2009.

[10] H. Wang, Y. Pei, A. LaLonde and G. Snyder, "Material design considerations based on thermoelectric quality factor," in *Thermoelectric Nanomaterials: Materials Design and Applications*, Berlin, Germany, Springer, 2013, pp. 3-33.

[11] R. Venkatasubramanian, E. Siivola, T. Colpitts and B. O'Quinn, "Thin-film thermoelectric devices with high room-temperature figures of merit," *Nature,* vol. 413, pp. 597-602, 2001.

[12] D. Rowe, V. Shukla and N. Savvides, "Phonon scattering at grain boundaries in heavily doped fine-grained silicon–germanium alloys," *Nature,* vol. 290, pp. 765-766, 1981.

[13] J. Vandersande, J. McCormack, J. Zoltan and J. Farmer, "Effect of neutron irradiation on the thermoelectric properties of SiGe alloys," Nevada, United States, 1990.

[14] J. Dismukes, L. Ekstrom, E. Steigmeier, I. Kudman and D. Beers, "Thermal and electrical properties of heavily doped Ge-Si alloys up to 1300°K," *Journal of Applied Physics,* vol. 35, no. 10, pp. 2899-2907, 1964.

[15] A. Boukai, Y. Bunimovich, J. Tahir-Kheli, J. Yu, W. Goddard and J. Heath, "Silicon nanowires as efficient thermoelectric materials," *Nature,* vol. 451, pp. 168-171, 2007.

[16] J. Dismukes, L. Ekstrom, E. Steigmeier, I. Kudman and D. Beers, "Thermal and Electrical Properties of Heavily Doped Ge-Si Alloys up to 1300°K," *Journal of Applied Physics,* vol. 35, no. 10, pp. 2899-2908, 1964.

[17] L. Hicks and M. Dresselhaus, "Thermoelectric figure of merit of a one-dimensional conductor," *Physical review B,* vol. 47, no. 24, p. 16631, 1993.

[18] J. Woodyard, "Nonlinear circuit device utilizing germanium". United States of America Patent US2530110 A, 14 November 1950.

[19] R. Venkatasubramanian, E. Siivola, T. Colpitts and B. O'Quinn, "Thin-film thermoelectric devices with high room-temperature figures of merit," *Nature,* vol. 413, pp. 597-602, 2001.

[20] A. Matoba, H. Watase, M. Kitai and K. Sasaki, "Investigation of thermoelectric properties of Si/Ge multilayer with ultra-heavily B doping," *Materials Transactions,* vol. 49, no. 8, pp. 1723-1727, 2008.

[21] X. Shi, Z. Zamanipour, J. Krasinski, A. Tree and D. Vashaee, "An investigation of electrical contacts for Higher Manganese Silicide," *Journal of Electronic Materials,* vol. 41, no. 9, pp. 2331-2337, 2012.

[22] D. Vashaee, J. Christofferson, Y. Zhang, A. Shakouri, G. Zeng, C. LaBounty, X. Fan, J. Piprek, J. Bowers and E. Croke, "Modeling and optimization of single-element bulk SiGe thin-film coolers," *Microscale Thermophysical Engineering,* vol. 9, no. 1, pp. 99-118, 2005.

[23] C.-H. Wu and R. Bube, "Thermoelectric and photothermoelectric effects in semiconductors: Cadmium sulfide films," *Journal of Applied Physics,* vol. 45, no. 2, pp. 648-661, 1974.

[24] F. Villani, P. Vacca, G. Nenna, O. Valentino, G. Burrasca, T. Fasolino, C. Minarini

and D. Della Sala, "Inkjet printed polymer layer on flexible substrate for OLED applications," *Journal of Physical Chemistry C,* vol. 113, no. 30, pp. 13398-13402, 2009.

[25] H. Haverinen, R. Myllylä and G. Jabbour, "Inkjet printing of light emitting quantum dots," *Applied Physics Letters,* vol. 94, no. 7, p. 073108, 2009.

[26] S. Horii, M. Sakurai, T. Uchikoshi, R. Funahashi, T. Suzuki, Y. Sakka, H. Ogino, J.-I. Shimoyama and K. Kishio, "Fabrication of multi-layered thermoelectric thick films and their thermoelectric performance," *Key Engineering Materials,* vol. 4112, pp. 291-296, 2009.

[27] M. Sakurai, S. Horii, R. Funahashi, T. Uchikoshi, T. Suzuki, Y. Sakka, H. Ogino, J.-I. Shimoyama and K. Kishio, "Improvement of thermoelectric properties of p- and n-type oxide thick films fabricated by electrophoretic deposition," *Materials Research Society Symposia Proceedings,* vol. 1044, no. 1044-U09-01, pp. 357-362, 2007.

[28] T. Okamoto, S. Horii, T. Uchikoshi, T. Suzuki, Y. Sakka, R. Funahashi, N. Ando, M. Sakurai, J.-I. Shimoyama and K. Kishio, "Fabrication of multilayered oxide thermoelectric modules by electrophoretic deposition under high magnetic fields," *Applied Physics Letters,* vol. 89, no. 8, p. 081912, 2006.

[29] A. Nozariasbmarz, A. Tahmasbi Rad, Z. Zamanipour, J. Krasinski, L. Tayebi and D. Vashaee, "Enhancement of thermoelectric power factor of silicon germanium films grown by electrophoresis deposition," *Scripta Materialia,* vol. 69, no. 7, pp. 549-552, 2013.

[30] L. Besra and M. Liu, "A review on fundamentals and applications of electrophoretic deposition (EPD)," *Progress in Materials Science,* no. 52, pp. 1-61, 2007.

[31] T. Yoshioka, A. Chávez-Valdez, J. Roether, D. Schubert and A. Boccaccini, "AC electrophoretic deposition of organic–inorganic composite coatings," *Journal of Colloid and Interface Science,* vol. 392, pp. 167-171, 2013.

[32] A. Gardeshzadeh, B. Raissi and E. Marzbanrad, "Electrophoretic deposition of SnO2 nanoparticles using low frequency AC electric fields," *Materials Letters,* vol. 62, no. 10-11, pp. 1697-1699, 2008.

[33] P. Sarkar, D. De, T. Uchikochi and L. Besra, "Electrophoretic Deposition (EPD): Fundamentals and novel applications in fabrication of advanced ceramic microstructures," in *Electrophoretic Deposition of Nanomaterials*, New York,

United States, Springer, 2012, pp. 181-215.

[34] W. Pickard, "Remarks on the theory of electrophoretic deposition," *Journal of The Electrochemical Society,* vol. 115, no. 4, pp. 105-108, 1933.

[35] P. Sarkar and P. Nicholson, "Electrophoretic deposition (EPD): mechanism, kinetics and application to ceramics," *Journal of the American Ceramic Society,* vol. 79, no. 8, pp. 1987-2002, 1996.

[36] E. Harsanyi, "Method of coating radiant bodies". United States of America Patent 1,897,902, 14 February 1933.

[37] T. Blickwedel and W. Rhyne, "Cataphoretically coated heater insulator assembly". United States of America Patent 2,831,140, 15 April 1958.

[38] F. Tang, T. Uchikoshi and Y. Sakka, "Electrophoretic deposition behavior of aqueous nanosized zinc oxide suspensions," *Journal of the American Ceramic Society,* vol. 85, no. 9, pp. 2161-2165, 2002.

[39] L. Besra, T. Uchikoshi, T. Suzuki and Y. Sakka, "Bubble-free aqueous electrophoretic deposition (EPD) by pulse potential application," *Journal of the American Ceramic Society,* vol. 91, no. 10, pp. 3154-3159, 2008.

[40] L. Besra, T. Uchikoshi, T. Suzuki and Y. Sakka, "Application of constant current pulse to suppress bubble incorporation and control deposit morphology during aqueous electrophoretic deposition (EPD)," *Journal of the European Ceramic Society,* vol. 29, no. 10, pp. 1837-1845, 2009.

[41] J. V. Tassel and C. Randall, "Mechanisms of electrophoretic deposition," *Key Engineering Materials,* vol. 314, pp. 167-174, 2006.

[42] J. V. Tassel and C. Randall, "Electrophoretic deposition and sintering of thin/thick PZT films," *Journal of the European Ceramic Society,* vol. 19, no. 6-7, pp. 955-958, 1999.

[43] J. V. Tassel and C. Randall, "Potential for integration of electrophoretic deposition into electronic device manufacture; demonstrations using silver/palladium," *Journal of Materials Science,* vol. 39, no. 3, pp. 867-879, 2004.

[44] H. Hamaker, "Formation of deposition by electrophoresis," *Transactions of the Faraday Society,* vol. 35, pp. 279-287, 1940.

[45] H. Hamaker and E. Verwey, "Colloid stability: the role of the forces between the particles in the electrodeposition and other phenomena," *Transactions of the Faraday Society,* vol. 35, pp. 180-185, 1940.

[46] P. Sarkar, X. Huang and P. Nicholson, "Electrophoretic deposition and its use to synthesize YSZ/A1203 micro laminate ceramic/ceramic composites," *Ceramic Engineering and Science Proceedings,* vol. 14, pp. 707-726, 1993.

[47] H. Koelmans and J. Overbeek, "Stability and electrophoretic deposition of suspensions in non-aqueous media," *Discussions of the Faraday Society,* vol. 18, pp. 52-63, 1954.

[48] B. Ferrari and R. Moreno, "The conductivity of aqueous Al2O3 slips for electrophoretic deposition," *Materials Letters,* vol. 28, pp. 353-355, 1996.

[49] H. Negishi, H. Yanagishita and H. Yokokawa, "Electrophoretic deposition of solid oxide fuel cell material powders," *Proceedings of the electrochemical society on electrophoretic deposition: fundamentals and applications,* vol. 21, pp. 214-221, 2002.

[50] L. Vandeperre, O. V. D. Biest and W. Clegg, "Silicon carbide laminates with carbon interlayers by electrophoretic deposition," *Key Engineering Materials,* vol. 1, pp. 127-131, 1997.

[51] R. Basu, C. Randall and M. Mayo, "Fabrication of dense zirconia electrolyte films for tubular solid oxide fuel cells by electrophoretic deposition," *Journal of American Ceramic Society,* vol. 84, pp. 33-40, 2001.

[52] T. Ishihara, K. Shimise, T. Kudo, H. Nishiguchi, T. Akbay and Y. Takita, "Preparation of Yttria-stabilised zirconia thin-films on strontium doped LaMnO3 cathode substrate via Electrophoretic," *Journal of the American Ceramic Society,* vol. 83, no. 8, pp. 1921-1927, 2000.

[53] A. Boccaccini and I. Zhitomirsky, "Application of electrophoretic and electrolytic deposition techniques in ceramics processing," *Current Opinion in Solid State and Materials Science,* vol. 6, no. 3, pp. 251-260, 2002.

[54] M. Gani, "Electrophoretic deposition: A review," *Industrial Ceramics,* vol. 14, pp. 163-174, 1994.

[55] O. V. d. Biest and L. Vandeperre, "Electrophoretic deposition of materials," *Annual Review of Materials Science,* vol. 29, pp. 327-352, 1999.

[56] T. Uchikoshi, T. Suzuki, F. Tang, H. Okuyama and Y. Sakka, "Crystalline-oriented TiO2 fabricated by the electrophoretic deposition in a strong magnetic field," *Ceramics International,* vol. 30, no. 7, pp. 1975-1978, 2004.

[57] T. Uchikoshi, T. Suzuki, S. Iimura, F. Tang and Y. Sakka, "Control of crystalline texture in polycrystalline TiO2 (Anatase) by electrophoretic deposition in a strong

magnetic field," *Journal of the European Ceramic Society,* vol. 26, no. 4-5, pp. 559-563, 2006.

[58] P. d. Rango, M. Lees, P. Lejay, A. Sulpice, R. Tournier, M. Ingold, P. Germi and M. Pernet, "Texturing of magnetic materials at high temperature by solidification in a magnetic field," *Nature,* vol. 349, pp. 770-772, 1991.

[59] L. Zhang, J. Vleugels and O. V. d. Biest, "Fabrication of textured alumina by orienting template particles during electrophoretic deposition," *Journal of the European Ceramic Society,* vol. 30, no. 5, pp. 1195-1202, 2010.

[60] H. Sarraf, L. Škarpová and P. Louda, "Influence of different anionic polyelectrolyte dispersants on the rheological and electrokinetic properties of carbon nanotubes," *Annual Transactions of the Nordic Rheology Society,* vol. 15, pp. 1-4, 2007.

[61] T. Suzuki, T. Uchikoshi, H. Okuyama, Y. Sakka and K. Hiraga, "Mechanical properties of textured, multilayered alumina produced using electrophoretic deposition in a strong magnetic field," *Journal of The European Ceramic Society,* vol. 26, no. 4, pp. 661-665, 2006.

[62] E. Askaria, M. Mehralib, I. Metselaara, N. Kadrib and M. Rahmana, "Fabrication and mechanical properties of Al2O3/SiC/ZrO2 functionally graded material by electrophoretic deposition," *Journal of the Mechanical Behavior of Biomedical Materials,* vol. 12, pp. 144-150, 2012.

[63] B. Ferrari, A. Bartret and C. Baudín, "Sandwich materials formed by thick alumina tapes and thin-layered alumina–aluminium titanate structures shaped by EPD," *Journal of the European Ceramic Society,* vol. 29, no. 6, pp. 1083-1092, 2009.

[64] B. Dzepina, I. Sigalas, M. Herrmann and R. Nilen, "The aqueous electrophoretic deposition (EPD) of diamond–diamond laminates," *International Journal of Refractory Metals and Hard Materials,* vol. 36, pp. 126-129, 2013.

[65] S. Suresh and A. Mortensen, "Functionally graded metals and metal–ceramic composites: part 2 thermomechanical behaviour," *International Materials Reviews,* vol. 42, no. 3, pp. 85-116, 1997.

[66] S. Bueno and C. Baudín, "Layered materials with high strength and flaw tolerance based on alumina and aluminium titanate," *Journal of the European Ceramic Society,* vol. 27, no. 2-3, pp. 1455-1462, 2007.

[67] B. Raissi, E. Marzbanrad and A. Gardeshzadeh, "Particle size separation by alternating electrophoretic deposition," *Journal of the European Ceramic Society,* vol. 29, no. 15, pp. 3289-3291, 2009.

[68] A. Boccaccini, J. Cho, T. Subhani, C. Kaya and F. Kaya, "Electrophoretic deposition of carbon nanotube–ceramic nanocomposites," *Journal of the European Ceramic Society,* vol. 30, no. 5, pp. 1115-1129, 2010.

[69] L. Wang, Y. Chen, T. Chen, W. Que and Z. Sun, "Optimization of field emission properties of carbon nanotubes cathodes by electrophoretic deposition," *Materials Letters,* vol. 61, no. 4-5, pp. 1265-1269, 2007.

[70] M. Ata, Y. Sun, X. Li and I. Zhitomirsky, "Electrophoretic deposition of graphene, carbon nanotubes and composites using aluminon as charging and film forming agent," *Colloids and Surfaces A: Physicochemical and Engineering Aspects,* vol. 398, pp. 9-16, 2012.

[71] F. Chicatun, J. Cho, S. Schaab, G. Brusatin, P. Colombo and J. Roether, "Carbon nanotube deposits and CNT/SiO2 composite coatings by electrophoretic deposition," *Advances in Applied Ceramics,* vol. 106, no. 4, pp. 186-195, 2007.

[72] S. Lee and W. Sigmund, "Formation of anatase TiO2 nanoparticles on carbon nanotubes," *Chemical Communications,* no. 6, pp. 780-781, 2003.

[73] A. Jitianu, T. Cacciaguerra, R. Benoit, S. Delpeux, F. Béguin and S. Bonnamy, "Synthesis and characterization of carbon nanotubes–TiO2 nanocomposites," *Carbon,* vol. 42, no. 5-6, pp. 1147-1151, 2004.

[74] J. Li and I. Zhitomirsky, "Electrophoretic deposition of manganese dioxide-carbon nanotube composites," *Journal of Materials Processing Technology,* vol. 209, no. 7, pp. 3452-3459, 2009.

[75] S. Mahajan, S. Hasan, J. Cho, M. Shaffer and A. Boccaccini, "Carbon nanotube–nanocrystal heterostructures fabricated by electrophoretic deposition," *Nanotechnology,* vol. 19, no. 19, p. 195301, 2008.

[76] A. White and S. Best, "Hydroxyapatite–Carbon nanotube composites for biomedical applications: A review," *International Journal of Applied Ceramic Technology,* vol. 4, no. 1, pp. 1-13, 2007.

[77] Y. Chen, Y. Zhang, T. Zhang, C. Gan, C. Zheng and G. Yu, "Carbon nanotube reinforced hydroxyapatite composite coatings produced through laser surface alloying," *Carbon,* vol. 44, no. 1, pp. 37-45, 2006.

[78] J. Ma, C. Wang and K. Peng, "Electrophoretic deposition of porous hydroxyapatite scaffold," *Biomaterials,* vol. 24, no. 20, pp. 3505-3510, 2003.

[79] A. Boccaccini, F. Chicatun, J. Cho, O. Bretcanu, J. Roether, S. Novak and Q. Chen, "Carbon nanotube coatings on bioglass-based tissue engineering scaffolds,"

Advanced Functional Materials, vol. 17, no. 15, pp. 2815-2822, 2007.

[80] B. Harrison and A. Atala, "Carbon nanotube applications for tissue engineering," *Biomaterials,* vol. 28, no. 2, pp. 344-353, 2007.

[81] Q. Li, X. Wang and D. Yuan, "Preparation of solid-phase microextraction fiber coated with single-walled carbon nanotubes by electrophoretic deposition and its application in extracting phenols from aqueous samples," *Journal of Chromatography A,* vol. 1216, no. 9, pp. 1305-1311, 2009.

[82] W. Chiu, K. Lee and W. Hsieh, "High efficiency flexible dye-sensitized solar cells by multiple electrophoretic depositions," *Journal of Power Sources,* vol. 196, no. 7, pp. 3683-3687, 2011.

[83] M. Hamadanian, A. Gravand and V. Jabbari, "High performance dye-sensitized solar cells (DSSCs) achieved via electrophoretic technique by optimizing of photoelectrode properties," *Materials Science in Semiconductor Processing,* vol. 16, no. 5, pp. 1352-1359, 2013.

[84] C. Chen, M. Wang, J. Li, N. Pootrakulchote, L. Alibabaei, C. Ngoc-le, J. Decoppet, J. Tsai, C. Gratzel, C. Wu, S. Zakeeruddin and M. Gratzel, "Highly efficient light-harvesting ruthenium sensitizer for thin-film dye-sensitized solar cells," *ACS Nano,* vol. 3, no. 10, pp. 3103-3109, 2009.

[85] T. Muroga, M. Gasparotto and S. Zinkle, "Overview of materials research for fusion reactors," *Fusion Engineering and Design,* Vols. 61-62, pp. 13-25, 2002.

[86] A. Tavassoli, "Present limits and improvements of structural materials for fusion reactors – A review," *Journal of Nuclear Materials,* vol. 302, no. 2-3, pp. 73-88, 2002.

[87] S. Novak, K. Rade, K. Konig and A. Boccaccini, "Electrophoretic deposition in the production of SiC/SiC composites for fusion reactor applications," *Journal of the European Ceramic Society,* vol. 28, no. 14, pp. 2801-2807, 2008.

[88] G. Niklasson and C. Granqvist, "Electrochromics for smart windows: Thin films of tungsten oxide and nickel oxide, and devices based on these," *Journal of Materials Chemistry,* vol. 17, no. 2, pp. 127-156, 2007.

[89] A. Subrahmanyam and A. Karuppasamy, "Optical and electrochromic properties of oxygen sputtered tungsten oxide (WO3) thin films," *Solar Energy Materials and Solar Cells,* vol. 91, no. 4, pp. 266-274, 2007.

[90] E. Khoo, P. Lee and J. Ma, "Electrophoretic deposition (EPD) of WO3 nanorods for electrochromic application," *Journal of the European Ceramic Society,* vol. 30,

no. 5, pp. 1139-1144, 2010.

[91] M. Verde, M. Peiteado, A. Caballero, M. Villegas and B. Ferrari, "Electrophoretic deposition of transparent ZnO thin films from highly stabilized colloidal suspensions," *Journal of Colloid and Interface Science,* vol. 373, no. 1, pp. 27-33, 2012.

[92] B. Ferrari, R. Moreno, L. Hernan, M. Melero, J. Morales and A. Caballero, "EPD of thick films for their application in lithium batteries," *Journal of the European Ceramic Society,* vol. 27, no. 13-15, pp. 3823-3827, 2007.

[93] J. Souquet and M. Duclot, "Thin film lithium batteries," *Solid State Ionics,* vol. 148, no. 3-4, pp. 375-379, 2002.

[94] J. Miller and A. Burke, "Electrochemical capacitors: challenges and opportunities for real-world applications," *The Electrochemical Society Interface,* vol. 17, no. 1, pp. 53-57, 2008.

[95] P. Sharma and T. Bhatti, "A review on electrochemical double-layer capacitors," *Energy Conversion and Management,* vol. 51, no. 12, pp. 2901-2912, 2010.

[96] L. Deng, Z. Hao, J. Wang, G. Zhu, L. Kang, Z. Liu, Z. Yang and Z. Wang, "Preparation and capacitance of graphene/multiwall carbon nanotubes/MnO2 hybrid material for high-performance asymmetrical electrochemical capacitor," *Electrochimica Acta,* vol. 89, pp. 191-198, 2013.

[97] J. Jang, K. Machida, Y. Kim and K. Naoi, "Electrophoretic deposition (EPD) of hydrous ruthenium oxides with PTFE and their supercapacitor performances," *Electrochimica Acta,* vol. 52, no. 4, pp. 1733-1741, 2006.

[98] C. Chen, S. Wang, C. Lin, F. Chen and C. Lin, "Electrophoretically deposited manganese oxide coatings for supercapacitor application," *Ceramics International,* vol. 35, no. 8, pp. 3469-3474, 2009.

[99] N. Minh, "Ceramic fuel cells," *Journal of the American Ceramic Society,* vol. 76, no. 3, pp. 563-588, 1993.

[100] J. Huijsmans, "Ceramics in solid oxide fuel cells," *Current Opinion in Solid State and Materials Science,* vol. 5, no. 4, pp. 317-323, 2001.

[101] N. Minh, "Solid oxide fuel cell technology—features and applications," *Solid State Ionics,* vol. 174, no. 1-4, pp. 271-277, 2004.

[102] C. Sun and U. Stimming, "Recent anode advances in solid oxide fuel cells," *Journal of Power Sources,* vol. 171, no. 2, pp. 247-260, 2007.

[103] S. Badwal and K. Foger, "Solid oxide electrolyte fuel cell review," *Ceramics International,* vol. 22, no. 3, pp. 257-265, 1996.

[104] H. Yokokawa, H. Tu, B. Iwanschitz and A. Mai, "Fundamental mechanisms limiting solid oxide fuel cell durability," *Journal of Power Sources,* vol. 182, no. 2, pp. 400-412, 2008.

[105] B. Zhu, "Functional ceria–salt-composite materials for advanced ITSOFC applications," *Journal of Power Sources,* vol. 114, no. 1, pp. 1-9, 2003.

[106] T. Talebi, B. Raissi, M. Haji and A. Maghsoudipour, "The role of electrical conductivity of substrate on the YSZ film formed by EPD for solid oxide fuel cell applications," *International Journal of Hydrogen Energy,* vol. 35, no. 17, pp. 9405-9410, 2010.

[107] T. Ishihara, K. Sato and Y. Takita, "Electrophoretic deposition of Y2O3-stabilized ZrO2 electrolyte films in solid oxide fuel cells," *Journal of the American Ceramic Society,* vol. 79, no. 4, pp. 913-919, 1996.

[108] T. Ishihara, K. Sato, Y. Mizuhara and Y. Takita, "Preparation of yttria-stabilized zirconia films for solid oxide fuel cells by electrophoretic deposition method," *Chemistry Letters,* vol. 21, no. 6, pp. 943-946, 1992.

[109] H. Konno, M. Tokita, A. Furusaki and R. Furuichi, "Electrochemical formation of a-site substituted perovskite structure La1−xMxCrO3 oxide coatings," *Electrochimica Acta,* vol. 37, no. 13, pp. 2421-2426, 1992.

[110] I. Zhitomirsky and A. Petric, "Electrolytic and electrophoretic deposition of CeO2 films," *Materials Letters,* vol. 40, no. 6, pp. 263-268, 1999.

[111] I. Zhitomirsky and A. Petric, "Electrolytic deposition of Gd2O3 and organoceramic composite," *Materials Letters,* vol. 42, no. 5, pp. 273-279, 2000.

[112] L. Jia, Z. Lü, X. Huang, Z. Liu, K. Chen, X. Sha, G. Li and W. Su, "Preparation of YSZ film by EPD and its application in SOFCs," *Journal of Alloys and Compounds,* vol. 424, no. 1-2, pp. 299-303, 2006.

[113] F. Chen and M. Liu, "Preparation of yttria-stabilized zirconia (YSZ) films on La0.85Sr0.15MnO3 (LSM) and LSM–YSZ substrates using an electrophoretic deposition (EPD) process," *Journal of the European Ceramic Society,* vol. 21, no. 2, pp. 127-134, 2001.

[114] I. Sora, R. Pelosato, A. Simone, L. Montanaro, F. Maglia and G. Chiodelli, "Characterization of LSGM films obtained by electrophoretic deposition (EPD)," *Solid State Ionics,* vol. 177, no. 19-25, pp. 1985-1989, 2006.

[115] I. Zhitomirsky and A. Petric, "Electrophoretic deposition of ceramic materials for fuel cell applications," *Journal of the European Ceramic Society,* vol. 20, no. 12, pp. 2055-2061, 2000.

[116] N. Priyantha, P. Jayaweera, A. Sanjurjo, K. Lau, F. Lu and K. Krist, "Corrosion-resistant metallic coatings for applications in highly aggressive environments," *Surface and Coatings Technology,* Vols. 163-164, pp. 31-36, 2003.

[117] M. El-Sharif, Y. Su, C. Chisholm and A. Watson, "Corrosion resistance of electrodeposited zinc-chromium alloy coatings," *Corrosion Science,* vol. 35, no. 5-8, pp. 1259-1265, 1993.

[118] P. O'Donnell, "Beryllium fluoride coating as a corrosion retardant for beryllium," *Corrosion Science,* vol. 7, no. 10, pp. 717-718, 1967.

[119] A. Pepe, M. Aparicio, S. Ceré and A. Durán, "Synthesis of hybrid silica sol–gel coatings containing Zn particles on carbon steel and Al/Zn coated carbon steel," *Materials Letters,* vol. 59, no. 29-30, pp. 3937-3940, 2005.

[120] A. Pepe, P. Galliano, S. Ceré, M. Aparicio and A. Durán, "Hybrid silica sol–gel coatings on Austempered Ductile Iron (ADI)," *Materials Letters,* vol. 59, no. 17, pp. 2219-2222, 2005.

[121] Y. Castro, B. Ferrari, R. Moreno and A. Durán, "Corrosion behaviour of silica hybrid coatings produced from basic catalysed particulate sols by dipping and EPD," *Surface and Coatings Technology,* vol. 191, no. 2-3, pp. 228-235, 2005.

[122] H. Lu, Y. Hu, M. Gu, S. Tang, H. Lu and X. Meng, "Synthesis and characterization of silica–acrylic–epoxy hybrid coatings on 430 stainless steel," *Surface and Coatings Technology,* vol. 204, no. 1-2, pp. 91-98, 2009.

[123] Y. Castro, B. Ferrari, R. Moreno and A. Durán, "Corrosion behaviour of silica hybrid coatings produced from basic catalysed particulate sols by dipping and EPD," *Surface and Coatings Technology,* vol. 191, no. 2-3, pp. 228-235, 2005.

[124] K. Kanamura and J. Hamagami, "Innovation of novel functional material processing technique by using electrophoretic deposition process," *Solid State Ionics,* vol. 172, no. 1-4, pp. 303-308, 2004.

[125] A. Boccaccini, U. Schindler and H. Krüger, "Ceramic coatings on carbon and metallic fibres by electrophoretic deposition," *Materials Letters,* vol. 51, no. 3, pp. 225-230, 2001.

[126] L. Kreethawate, S. Larpkiattaworn, S. Jiemsirilers, L. Besra and T. Uchikoshi, "Application of electrophoretic deposition for inner surface coating of porous

ceramic tubes," *Surface and Coatings Technology*, vol. 205, no. 7, pp. 1922-1928, 2010.

[127] R. d. A. Franchini, C. d. Souza, R. Colombara, M. C. Matos and R. Matos, "Rapid determination of hydrogen peroxide using peroxidase immobilized on Amberlite IRA-743 and minerals in honey," *Journal of Agricultural and Food Chemistry,* vol. 55, no. 17, pp. 6885-6890, 2007.

[128] N. Dougami and T. Takada, "Modification of metal oxide semiconductor gas sensor by electrophoretic deposition," *Sensors and Actuators B: Chemical,* vol. 93, no. 1-3, pp. 316-320, 2003.

[129] G. Korotcenkov, "Gas response control through structural and chemical modification of metal oxide films: state of the art and approaches," *Sensors and Actuators B: Chemical,* vol. 107, no. 1, pp. 209-232, 2005.

[130] N. Han, P. Deng, J. Chen, L. Chai, H, Gao and Y. Chen, "Electrophoretic deposition of metal oxide films aimed for gas sensors application: The role of anodic aluminum oxide (AAO)/Al composite structure," *Sensors and Actuators B: Chemical,* vol. 144, no. 1, pp. 267-273, 2010.

[131] F. Hossein-Babaei and F. Taghibakhsh, "Electrophoretically deposited zinc oxide thick-film gas sensors," *Electronics Letters,* vol. 36, no. 21, pp. 1815-1816, 2000.

[132] T. King, M. Preston, B. Murphy and D. Cannell, "Piezoelectric ceramic actuators: A review of machinery applications," *Precision Engineering,* vol. 12, no. 3, pp. 131-136, 1990.

[133] E. Crawley and J. D. Luis, "Use of piezoelectric actuators as elements of intelligent structures," *The American Institute of Aeronautics and Astronautics Journal,* vol. 25, no. 10, pp. 1373-1385, 1987.

[134] X. Chao, Z. Yang, G. Li and Y. Cheng, "Fabrication and characterization of low temperature sintering PMN–PZN–PZT step-down multilayer piezoelectric transformer," *Sensors and Actuators A: Physical,* vol. 144, no. 1, pp. 117-123, 2008.

[135] S. Trolier-McKinstry and P. Muralt, "Thin film piezoelectrics for MEMS," *Journal of Electroceramics,* vol. 12, no. 1-2, pp. 7-17, 2004.

[136] W. Dong, L. Sun and Z. Du, "Design of a precision compliant parallel positioner driven by dual piezoelectric actuators," *Sensors and Actuators A: Physical,* vol. 135, no. 1, pp. 250-256, 2007.

[137] Y. Chen, J. Ma and T. Li, "Electrophoretic deposition and characterization of a

piezoelectric FGM monomorph actuator," *Ceramics International,* vol. 30, no. 7, pp. 1807-1809, 2004.

[138] Y. Chen, T. Li, F. Boey and J. Ma, "Electrophoretic deposition and characterization of helical piezoelectric actuator," *Ceramics International,* vol. 34, no. 1, pp. 1-6, 2008.

[139] D. Stojanovic, B. Jokic, D. Veljovic, R. Petrovic, P. Uskokovic and D. Janackovic, "Bioactive glass–apatite composite coating for titanium implant synthesized by electrophoretic deposition," *Journal of the European Ceramic Society,* vol. 27, no. 2-3, pp. 1595-1599, 2007.

[140] A. Boccaccini, S. Keim, R. Ma, Y. Li and I. Zhitomirsky, "Electrophoretic deposition of biomaterials," *Journal of the Royal Society Interface,* vol. 7, no. 5, pp. 581-613, 2010.

[141] L. Hench, "The story of bioglass," *Journal of Materials Science: Materials in Medicine,* vol. 17, no. 11, pp. 967-978, 2006.

[142] H. Kim, "Ceramic bioactivity and related biomimetic strategy," *Current Opinion in Solid State and Materials Science,* vol. 7, no. 4-5, pp. 289-299, 2003.

[143] I. Zhitomirsky and L. Gal-Or, "Electrophoretic deposition of hydroxyapatite," *Journal of Materials Science: Materials in Medicine,* vol. 8, no. 4, pp. 213-219, 1997.

[144] J. Roether, A. Boccaccini, L. Hench, V. Maquet, S. Gautier and R. Jerome, "Development and in vitro characterization of novel bioresorbable and bioactive composite materials based on polylactide foams and Bioglass® for tissue engineering applications," *Biomaterials,* vol. 23, no. 18, pp. 3871-3878, 2002.

[145] D. Stojanovic, B. Jokic, D. Veljovic, R. Petrovic, P. Uskokovic and D. Janackovic, "Bioactive glass–apatite composite coatings for titanium implant synthesized by electrophoretic deposition," *Journal of the European Ceramic Society,* vol. 27, no. 2-3, pp. 1595-1599, 2007.

[146] M. Javidi, S. Javadpour and M. Bahrololoom, "Electrophoretic deposition of natural hydroxyapatite on medical grade 316L stainless steel," *Materials Science and Engineering: C,* vol. 28, no. 8, pp. 1509-1515, 2008.

[147] X. Pang and I. Zhitomirsky, "Electrodeposition of composite hydroxyapatite–chitosan films," *Materials Chemistry and Physics,* vol. 94, no. 2-3, pp. 245-251, 2005.

[148] P. Wang, C. Li, H. Gong, X. Jiang, H. Wang and K. Li, "Effects of synthesis

conditions on the morphology of hydroxyapatite nanoparticles produced by wet chemical process," *Powder Technology,* vol. 203, no. 2, pp. 315-321, 2010.

[149] P. Ducheyne, S. Radin, M. Heughebaert and J. Heughebaert, "Calcium phosphate ceramic coatings on porous titanium: effects of structure and composition on electrophoretic deposition," *Biomaterials,* vol. 11, no. 4, pp. 244-254, 1990.

[150] M. Wei, A. Ruys, B. Milthorpe and C. Sorrel, "Solution ripening of hydroxyapatite nanoparticles: Effects on electrophoretic deposition," *Journal of Biomedical Materials Research Part A,* vol. 45, no. 1, pp. 11-19, 1999.

[151] J. Ma, C. Wang and K. Peng, "Electrophoretic deposition of porous hydroxyapatite scaffold," *Biomaterials,* vol. 24, no. 20, pp. 3505-3510, 2003.

[152] C. Wang, J. Ma, W. Cheng and R. Zhang, "Thick hydroxyapatite coatings by electrophoretic deposition," *Materials Letters,* vol. 57, no. 1, pp. 99-105, 2002.

[153] S. Mahmoodi, L. Sorkhi, M. Farrokhi-Rad and T. Shahrabi, "Electrophoretic deposition of hydroxyapatite–chitosan nanocomposite coatings in different alcohols," *Surface and Coatings Technology,* vol. 216, pp. 106-114, 2013.

[154] J. Jones, "Review of bioactive glass: From Hench to hybrids," *Acta Biomaterialia,* vol. 9, no. 1, pp. 4457-4486, 2013.

[155] L. Hench, "Bioceramics," *Journal of the American Ceramic Society,* vol. 81, no. 7, pp. 1705-1728, 1998.

[156] M. Mehdipour, A. Afshar and M. Mohebali, "Electrophoretic deposition of bioactive glass coating on 316L stainless steel and electrochemical behavior study," *Applied Surface Science,* vol. 258, no. 24, pp. 9832-9839, 2012.

[157] D. Zhitomirsky, J. Roether, A. Boccaccini and I. Zhitomirsky, "Electrophoretic deposition of bioactive glass/polymer composite coatings with and without HA nanoparticle inclusions for biomedical applications," *Journal of Materials Processing Technology,* vol. 209, no. 4, pp. 1853-1860, 2009.

[158] S. Yamaguchi, T. Yabutsuka, M. Hibino and T. Yao, "Development of novel bioactive composites by electrophoretic deposition," *Materials Science and Engineering: C,* vol. 29, no. 5, pp. 1584-1588, 2009.

[159] B. Neirinck, L. V. Mellaert, J. Fransaer, O. V. d. Biest, J. Anné and J. Vleugels, "Electrophoretic deposition of bacterial cells," *Electrochemistry Communications,* vol. 11, no. 9, pp. 1842-1845, 2009.

[160] M. Razavi, M. Fathi, O. Savabi, S. Razavi, B. Hashemi Beni, D. Vashaee and L.

Tayebi, "Controlling the degradation rate of bioactive magnesium implants by electrophoretic deposition of akermanite coating," *Ceramics International*, vol. 40, no. 3, pp. 3865-3872, 2013.

[161] N. Satyala, A. Tahmasbi Rad, Z. Zamanipour, P. Norouzzadeh, J. Krasinski, L. Tayebi and D. Vashaee, "Reduction of thermal conductivity of bulk nanostructured bismuth telluride composites embedded with silicon nano-inclusions," *Journal of Applied Physics*, vol. 115, no. 4, p. 044304, 2014.

[162] Z. Zamanipour, X. Shi, A. Dehkordi, J. Krasinski and D. Vashaee, "The effect of synthesis parameters on transport properties of nanostructured bulk thermoelectric p-type silicon germanium alloy," *Physica Status Solidi (a)*, vol. 209, no. 10, pp. 2049-2058, 2012.

[163] D. White and P. Klemens, "Thermal conductivity of thermoelectric Si0.8-Ge0.2 alloys," *Journal of Applied Physics*, vol. 71, no. 9, pp. 4258-4263, 1992.

[164] F. Geiger and F. Cunningham, "Ambipolar diffusion in semiconductors," *American Journal of Physics*, vol. 32, no. 5, pp. 336-342, 1964.

VITA

Pouya Amrollahi

Candidate for the Degree of

Master of Science

Thesis: DEVELOPMENT OF THERMOELECTRIC THICK-FILMS VIA ELECTROPHORETIC DEPOSITION

Major Field: Materials Science and Engineering

Biographical:

Education:

Completed the requirements for the Master of Science in Materials Science and Engineering at Oklahoma State University, Tulsa, Oklahoma in July, 2014.

Completed the requirements for the Bachelor of Science in Materials Science and Engineering at University of Tehran, Tehran, Iran in September, 2012.

Experience:

Characterization Methods: XRD, SEM, TEM, EDS, TMA, DTA, DSC, FTIR

Software: Office, PANalytical X'pert HighScore, EVA, Surface Analyzer, Image Analyzer, Inca, AZtec

Fabrication: Sputtering, Spin coating, Photolithography

Processing: Milling, Sol-gel, Microwave Sintering, Hot pressing